

## INTRODUCTION OF FLUORINE INTO COALS USING *N*-FLUOROBENZENESULFONIMIDE.

Edward W. Hagaman and Suk Kyu Lee  
Chemistry Division, Oak Ridge National Laboratory  
Oak Ridge, Tennessee 37831-6201

Keywords: *N*-fluorobenzenesulfonimide, DCP/MAS  $^{13}\text{C}$  NMR, fluorinated coal

### INTRODUCTION

The selective introduction of fluorine into coals is under study as part of a program to define the chemical reactivity of coals through identification of reactive functional groups in the organic matrix of these solid fossil fuels. Recently, the number of reactive sites in coals as function of the strength of the organic indicator base has been determined by the C-methylation of *O*-methylated coals (1,2). The C-methylation was carried out by treatment of coal with carbanion bases and quenched with  $^{13,14}\text{C}$  methyl iodide. The structural information derived from C-methylation of coals was limited to the number of reactive sites and an estimate of the methylene/methine site ratio (3). The generation of anions in coals is being repeated and quenched with *N*-fluorobenzenesulfonimide, 1, (4,5), a versatile electrophilic fluorinating reagent, in order to chemically attach fluorine to the reactive carbon site. The  $^{19}\text{F}$  nucleus provides the mechanism, dipole-dipole coupling, to selectively observe the  $^{13}\text{C}$  nuclei in its immediate vicinity through the use of  $^1\text{H}$ - $^{13}\text{C}$ - $^{19}\text{F}$  double cross polarization (DCP)/MAS  $^{13}\text{C}$  NMR. In conjunction with MAS  $^{19}\text{F}$  NMR and CP/MAS  $^{13}\text{C}$  NMR experiments, the goal is the definition of the reactive sites in sufficient detail to discover the chemical basis for the C-H acidity of the original carbanions.

### RESULTS AND DISCUSSION

*O*-methylated Illinois #6 coal was prepared by using tetrabutylammonium hydroxide and methyl iodide (2,6,7). The different anions of *O*-methylated Illinois #6 coal were prepared using fluorenyl lithium, *n*-butyl lithium, and lithium diisopropyl amine (LDA), respectively, in THF. Each of the coal anions prepared by different bases was quenched with 1 at  $-78^\circ\text{C}$ . The reaction mixture was slowly warmed to RT and stirred for an additional 15 hours under Argon. After addition of saturated  $\text{NH}_4\text{Cl}$ , the solution was diluted with 5% NaOH solution in order to destroy the excess 1. The coal was collected by filtration, and successively washed with water, 1N HCl, water, and ethanol. The coal was extracted exhaustively with THF using a Soxhlet extraction apparatus and then dried under vacuum for 18 hours at  $100^\circ\text{C}$ .

The  $^{19}\text{F}$  NMR spectrum of the fluorinated coal prepared using fluorenyl lithium and 1 shows a strong resonance at  $-123$  ppm and a less intense resonance around  $-170$  ppm (Figure 1). These resonances correspond to tertiary and secondary alkyl fluorides, respectively. The spectrum also contains a poorly resolved broad resonance at  $-100$  ppm. Associated with this center band are first and second order side bands that indicate a very large static linewidth

for this band. The linewidth and chemical shift of this band are the signature of *gem*-difluorocarbon species.

The difference spectrum between the CP/MAS-<sup>13</sup>C NMR spectra of the fluorinated coal prepared with fluorenyl lithium (Fig. 2a) and the O-methylated Illinois #6 precursor (Fig. 2b) is shown in Fig. 2c. Difference spectroscopy could show, in principal, the chemical shift reorganization due to the introduction of fluorine into the coal. In fact the difference spectrum is similar to the spectrum of fluorene, in the aromatic region, and indicates that the fluorenyl group is incorporated into the coal. The absence of the C(9) resonance of fluorene in the difference spectrum suggests the base is chemically attached to the coal network. The C(9) chemical shift will vary depending on the nature of the coal "substituent" at C(9), and will be distributed over a broad region. The remote aromatic carbons are less sensitive to the details of the bonding configuration at the *sp*<sup>3</sup> site. In control experiments it has been shown that physically absorbed fluorene can be completely removed by normal work-up procedures (Fig. 3). Hence, a fraction of the fluorenyl lithium reacts as a nucleophile and adds to O-methylated coal to give fluorenyl-coal linkages. These results support earlier work with [9-<sup>13</sup>C]-fluorenyllithium which show reagent-derived fluorene is chemically bound to the organic coal matrix (3).

The CP/MAS <sup>13</sup>C NMR of a fluorinated coal produced using *n*-butyl lithium and 1 reveals that the *n*-butyl group is also chemically grafted into the coal. This is evident from comparison of the aliphatic region of the resolution enhanced spectrum (upper trace in Fig. 4a) of this material with the corresponding region in the spectrum of the precursor coal (Fig. 2b). The resonance of the methyl group of the *n*-butyl moiety is quite insensitive to the nature of the attachment and appears as the sharp peak at 13 ppm. The spectrum in Fig. 2b does not show this resolved feature.

The CP/MAS <sup>13</sup>C NMR spectrum of the fluorinated coal produced using LDA and 1 is similar to that of the starting O-methylated Illinois #6 coal. The difference between these two spectra provides no evidence for *sec*-propyl amine resonances that would indicate nucleophilic addition of the base in the coal network.

While a necessary part of the background work to elucidate the chemical conversion occurring in the coal matrix the CP/MAS <sup>13</sup>C NMR spectra above do not reveal the fluorination chemistry the coal has undergone. This information is provided by the <sup>1</sup>H-<sup>13</sup>C-<sup>19</sup>F DCP/MAS <sup>13</sup>C NMR experiment (8). The DCP spectrum of the fluorinated coal prepared using fluorenyl lithium and 1 shows two kind of carbon resonances at 90-110 ppm and 150-170 ppm (Fig. 5). These resonances are assigned to alkyl fluoride carbons and aryl fluoride carbons, respectively. Aryl fluorides are formed by directed *ortho*-lithiation of activated aromatic rings (4).

The DCP/MAS <sup>13</sup>C NMR spectrum of the fluorinated coal prepared using *n*-butyl lithium and 1 (Fig. 4b) also shows aryl and alkyl fluoride resonance bands. The spectrum is similar to that of the fluorinated coal prepared with fluorenyl lithium and 1 (Fig. 5).

The DCP/MAS <sup>13</sup>C NMR spectrum of the fluorinated coal prepared using LDA and 1 shows only an aryl carbon resonance band.

## ACKNOWLEDGEMENT

Research sponsored by the Division of Chemical Sciences, Office of Basic Energy Sciences, U.S. Department of energy under contract DE-AC05-84OR21400 with Martin Marietta Energy Systems, Inc.

## REFERENCES

1. Hagaman, E. W., Chambers Jr., R. R., Woody, M. C., *Anal. Chem.*, 1986, **58**, 387.
2. Chambers Jr., R. R., Hagaman, E. W., Woody, M. C., Smith, K. E., McKamey, D.R., *Fuel*, 1985, **64**, 1349.
3. Hagaman, E. W., Chambers, R. R., Woody, M. C., *Energy & Fuels*, 1987, **1**, 352.
4. Differding, E., Ofner, H., *Synlett*. 1991, 187.
5. Differding, E., Ofner, H., *Synlett*. 1991, 395.
6. Liotta, R., Rose, K., Hippo, E. J., *Org. Chem.* 1981, **46**, 277.
7. Liotta, R., Brons, G. J., *Am. Chem. Soc.* 1981, **103**, 1735.
8. Hagaman, E. W., Burns, J. H., *Fuel* in press.

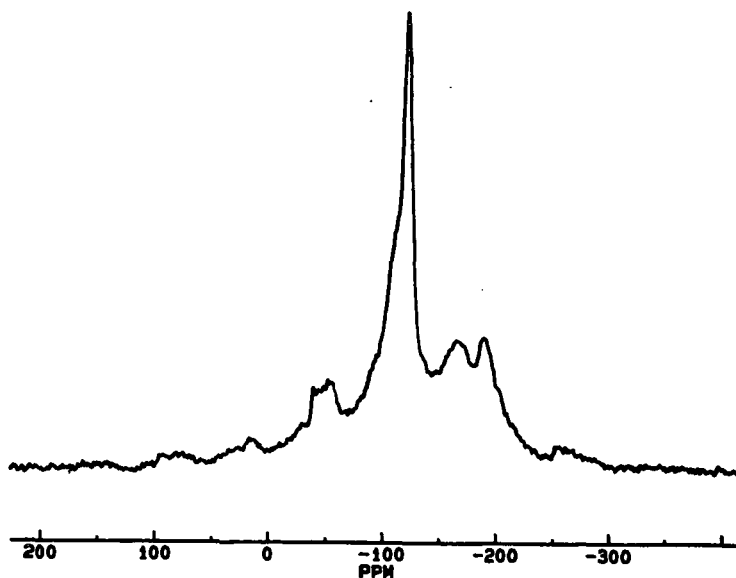


Fig. 1 MAS  $^{19}\text{F}$  spectrum of a fluorinated coal by reaction of O-methylated Illinois # 6 coal with fluorenyl lithium and N-fluorobenzenesulfonimide.

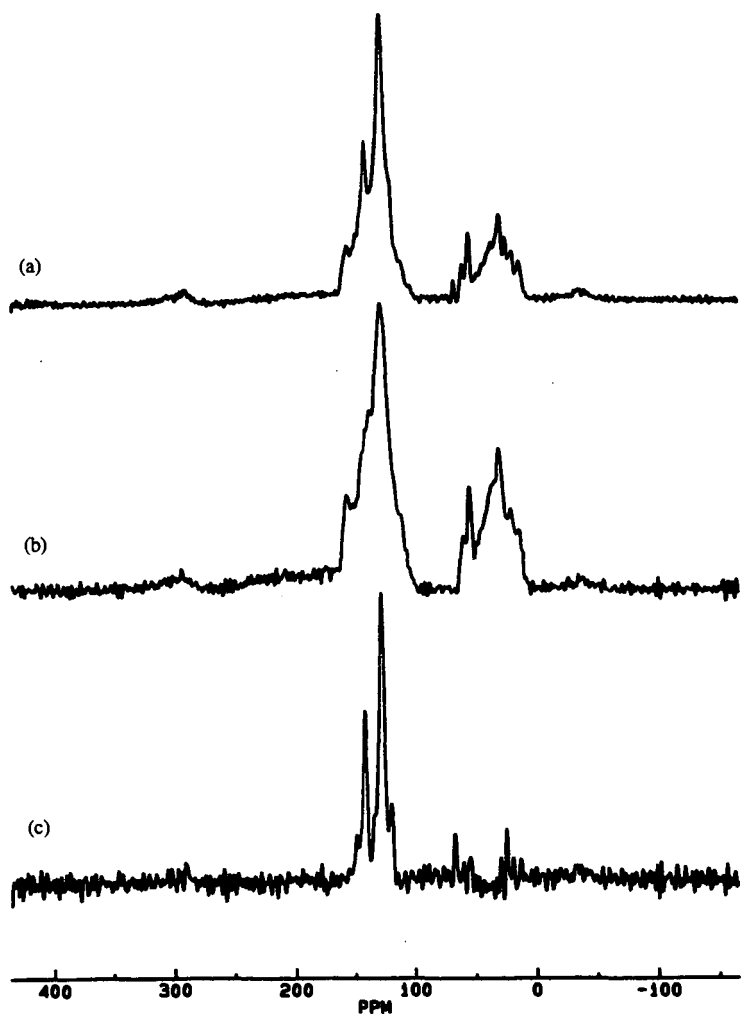


Fig. 2 (a) Resolution-enhanced CP/MAS  $^{13}\text{C}$  spectrum of a fluorinated coal by reaction of O-methylated Illinois # 6 coal with fluorenyl lithium and N-fluorobenzenesulfonimide.  
(b) Resolution-enhanced CP/MAS  $^{13}\text{C}$  spectrum of O-methylated Illinois # 6 coal.  
(c) Difference spectrum: (a) minus (b).

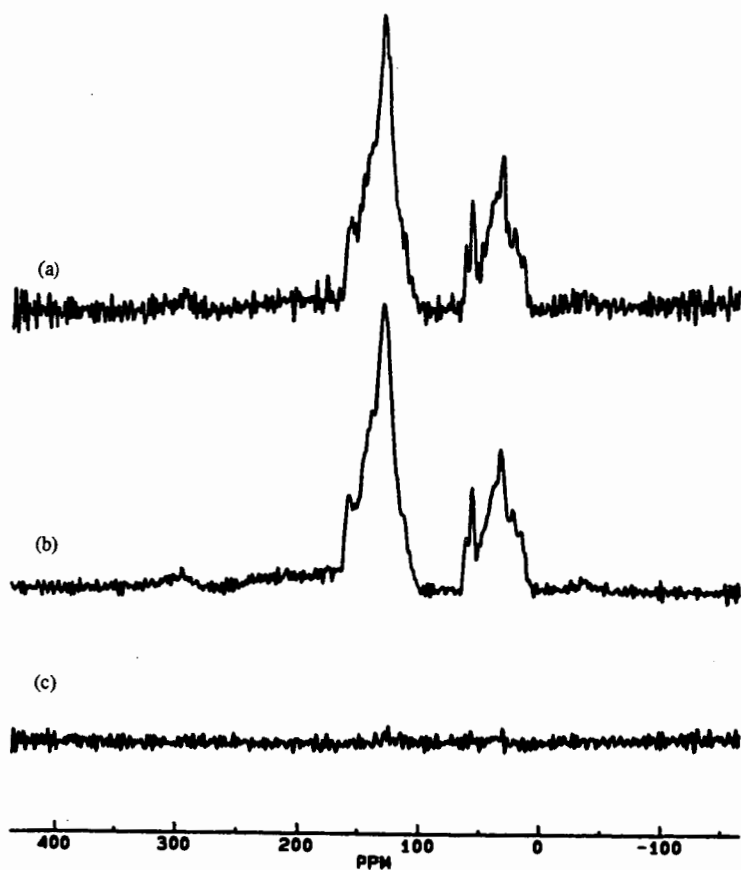


Fig. 3 (a) Resolution-enhanced CP/MAS  $^{13}\text{C}$  spectrum of O-methylated Illinois # 6 coal which has been treated with fluorene and THF for 18hrs. and then successively washed with 5% NaOH,  $\text{H}_2\text{O}$ , 1N HCl,  $\text{H}_2\text{O}$ , and ethanol followed by vacuum drying for 18hrs at  $100^\circ\text{C}$ . (b) Resolution-enhanced CP/MAS  $^{13}\text{C}$  spectrum of O-methylated Illinois # 6 APC coal. (c) Difference spectrum: (a) minus (b).

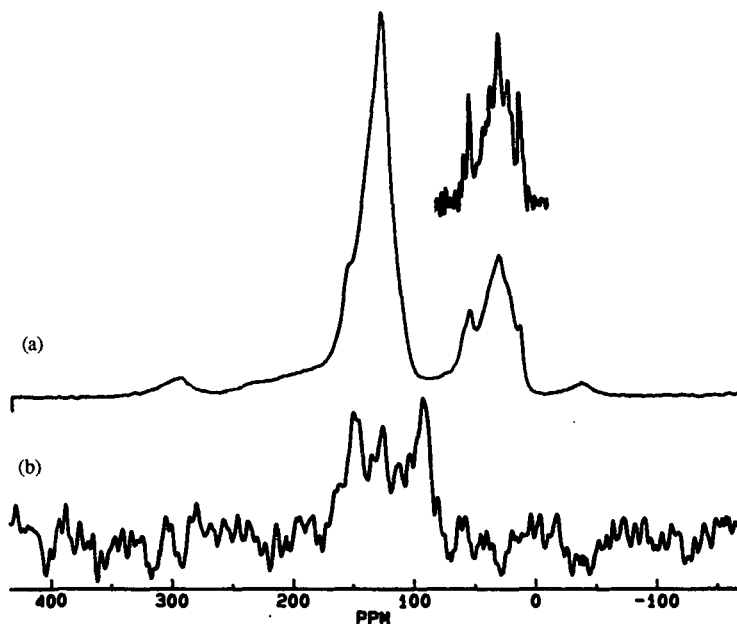


Fig. 4 (a) CP/MAS  $^{13}\text{C}$  spectrum of a fluorinated coal by reaction of O-methylated Illinois # 6 coal with n-butyl lithium and N-fluorobenzenesulfonimide. The aliphatic region of the resolution-enhanced spectrum is plotted above the full spectrum.  
 (b) DCP/MAS  $^{13}\text{C}$  spectrum of the same coal.

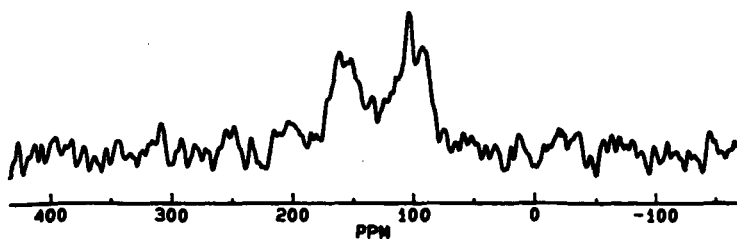


Fig. 5 DCP/MAS  $^{13}\text{C}$  spectrum of a fluorinated coal by reaction of O-methylated Illinois # 6 coal with fluorenyl lithium and N-fluorobenzenesulfonimide.

## NITROGEN XANES STUDIES OF FOSSIL FUELS.

Sudipa Mitra-Kirtley,<sup>a</sup> Oliver C. Mullins,<sup>b</sup> Jan Branthaver,<sup>c</sup> Jan van Elp,<sup>d</sup> and Stephen P. Cramer<sup>d,e</sup>

<sup>a</sup> Rose-Hulman Institute of Technology, Terre Haute, IN 47803,

<sup>b</sup> Schlumberger-Doll Research, Ridgefield, CT 06877,

<sup>c</sup> Western Research Institute, WY,

<sup>d</sup> Lawrence Berkeley Laboratory, Berkeley, CA 94720,

<sup>e</sup> University of California, Davis, CA 95616

Keywords: XANES, nitrogen, coals

All the major nitrogen chemical structures, present in coals of varying ranks have been quantitatively determined using nitrogen X-ray Absorption Near-Edge Spectroscopy (XANES). XANES spectra of these samples exhibit several distinguishable resonances which can be correlated with characteristic resonances of particular nitrogen chemical structures thereby facilitating analysis of these complicated systems. Aromatic nitrogen compounds abound in the coals; no evidence of saturated amine is found. Pyrroles, pyridines, pyridones, and aromatic amines are found in coal; of these, pyrrolic structures are the most prevalent. The low rank (high oxygen) coals have large quantities of pyridone and smaller quantities of pyridine; this suggests that with increasing maturation of coal, pyridone loses its oxygen and is transformed into pyridine. Aromatic amines are present at low levels in coals of all rank. Preliminary studies on kerogens and bitumens indicate the presence of pyrrole, pyridone, pyridine, and aromatic amine structures; some saturated amine may also be present. Other models containing multiple oxygen and nitrogen sites have been investigated and they may be present in bitumens and low rank coals in small quantities.

### INTRODUCTION

Coal is a valuable natural resource. The origin of the organic part of coal stems from plant materials, which over geological time, become compacted, and mature into coal beds due to severe physical conditions such as heat and pressure. Heteroatoms such as nitrogen and sulfur present in fossil fuels pose major problems in the effective usage of the resource. Heteroatoms in coals often act as catalyst poisons; upon combustion of coal, heteroatoms evolve gases which are harmful to the environment. Heteroatoms also help in the determination of solubility and chemical properties of coal. Heteroatoms also provide markers to follow evolution of the chemistry of coal with maturation.

The rank of coal by definition is a measure of the degree of metamorphism of coal beds, higher rank indicating greater maturation. During the process of maturation, moisture and chemically bound oxygen are expelled from coal beds, and consequently, higher rank coals have lower oxygen and moisture content than lower rank coals. Aromaticity increases with maturation; carbon aromaticity can range from 90% in a high rank coal to 40% in a low rank coal. Oxygen, which is the major heteroatom present in coals, occur as furan analogues, phenolic analogues, and etheric groups. Sulfur is present in coals both in aromatic and saturated forms. X-ray Absorption Near-Edge Structure (XANES) spectroscopy has been used for the last ten years to successfully determine the major sulfur chemical forms present in coals(1-4). Thiophenic (aromatic) sulfur is the dominant type, followed by sulfidic (saturated) type of sulfur. Oxygen containing sulfur forms such as sulfoxides, sulfones and sulfates are also found in coals, as well as mineral pyritic sulfur(2,4).

Kerogens are the organic insoluble, and bitumens are the organic soluble fractions of oil shales. The maturation process is somewhat similar to coal maturation; however, the maturation process of kerogen results in the production of crude oil. The H:C ratio of both immature kerogens and bitumens is typically ~1.5. Most of the carbon exists in aliphatic forms, and nitrogen and oxygen are present in greater amounts than sulfur.

Nitrogen has been difficult to study in fossil fuels; the high molecular weight of coals hinder chromatographic measurements, and the low concentrations of nitrogen in coal make spectroscopic measurements difficult. X-ray photoelectron studies in coal

have been informative, but the limited energy resolution hinders determination of all major forms of nitrogen(5,6). Nitrogen studies have also been difficult in kerogens and bitumens; insolubility of kerogens and complex structures of both kerogens and bitumens exacerbate the analysis of their nitrogen chemistry. XANES methodology is direct and nondestructive and has already been successful in determining the different nitrogen chemical functionalities in coal (7,8) and petroleum asphaltenes(9).

The present study determines all principal nitrogen structures of coals of varying ranks; this study has also been extended to provide preliminary information about immature kerogens and bitumens. Pyrrole and pyridine are found in these samples; in addition, presence of pyridones and aromatic amines, and very small amounts of saturated amines are also found. In the low rank coals, there is less or no pyridine but considerable amounts of pyridone; in the high rank coals the pyridones lose the oxygen and become converted into pyridines. Aromatic amines, and very small amounts of saturated amines are found in both the immature kerogens and bitumens. The XANES spectra of the kerogens and bitumens suggest the presence of pyrroles, pyridones, pyridines, and aromatic amines, and perhaps small amounts of saturated amines. During the maturation process of oil shales while some biomarkers remain unaltered, several starting chemical functionalities in immature oil shales alter significantly in the production of crude oil. Our present data on the immature kerogens and bitumens suggest that there may be considerable quantities of pyridone present in them; in that case, these structures disintegrate upon reaching the crude oil stage, as our previous studies on petroleum asphaltenes(9) did not show any occurrence of pyridone structures.

#### EXPERIMENTAL SECTION

Our nitrogen XANES data have been collected at beamline U4B at National Synchrotron Light Source at Brookhaven National Lab; this beamline has been constructed by AT&T Bell Labs(10). We used a monochromator consisting of a grating of 600 lines/mm, and a multi-element fluorescent Ge detector(11). The pressure inside the beampipe leading to the sample chamber, as well as the sample chamber was on the order of  $10^{-9}$ - $10^{-10}$  torr; a cryopump and a turbo-molecular pump were used to maintain such high vacuum conditions. Samples were placed on nitrogen-free Scotch tape and were positioned inside the chamber by means of a load-lock system.

Our sample suite consisted of several coals, kerogens, bitumens, and nitrogen model compounds. The coals were obtained from Argonne National Laboratory Coal Sample Bank, IL(12), the kerogens and the bitumens were obtained from Western Research Institute, WY, and the model compounds from Aldrich Chemical Company. The models were used as received, without any further purification.

#### RESULTS AND DISCUSSIONS

Figure 1 plots the nitrogen XANES of several coals of varying ranks; the plots are in the order of increasing rank from the bottom to the top of the figure. Three principal regions are noticed, at ~400 eV, 402-405 eV, and 408 eV; the second region can be decomposed into three regions, at 402 eV, 403.3 eV, and 405 eV. The first resonance region at 400 eV varies considerably in intensity among the different coals, the intensity gradually increases as we move from a lower rank coal to a higher rank coal. The resonance feature at 402 eV, on the other hand, grows in intensity as we move from a higher rank to a lower rank coal. This suggests that as coal matures, the nitrogen structure identifiable with the 402 eV resonance feature transforms into a structure whose characteristic resonance is at 400 eV. The resonance feature at 403.3 eV in all the spectra varies less dramatically within different samples, and the 405 eV resonance intensity is rather small for all the plots.

Figure 2 shows the XANES plots of several kerogens and bitumens. Here we notice the three distinct resonance regions also observed in the coal plots, where the second region can be decomposed into three features. The peaks at 400 eV and ~403 eV are well pronounced in all the kerogen and bitumen spectra, the feature slightly shifted from 402 eV is very well pronounced in the bitumens, and the exact origin of such a peak is still under investigation.

XANES plots of a high rank coal, a low rank coal, a kerogen, a bitumen and analogues of five different nitrogen structures are shown in figure 3. The first resonance in the fossil-fuel spectra match well with the  $\pi^*$  resonance of pyridine, suggesting the presence of pyridine in these samples. The second resonance feature in the fossil-fuel spectra matches well with  $\pi^*$  resonance energy of the pyridone molecule. This suggests the presence of such structures in the fossil-fuel samples. The spectrum of a high rank coal has an intense pyridine peak, but a barely discernible shoulder for the pyridone signature; the opposite situation exists in the spectrum of the low rank coal, where the pyridine peak is absent, and a strong pyridone peak is present. This leads to the argument that as coals mature, oxygen is driven away, and the pyridone in a low rank coal loses its oxygen when it reaches a high rank stage and is transformed into pyridine(8). Among the kerogen and bitumen, the peak around 402 eV is relatively strong; this may be partly due to the presence of pyridone structures, as well as other oxygen nitrogen structures, and the issue is still under investigation. The kerogen and bitumen samples are immature, and considerable amounts of pyridone, as well as other oxygen containing molecules are not unexpected to be present in these samples. The third resonance in the fossil-fuel spectra corresponds in energy with the  $\pi^*$  resonance of the pyrrole molecule. The four fossil-fuel samples show intense pyrrole resonances, and the intensity is more or less uniform in all the four spectra. The smaller resonance feature at 405 eV in the fossil-fuel spectra can be attributed to the presence of aromatic amines, since the spectrum of an amine has a broad resonance in this region. The saturated amine spectrum shows an absence of a  $\pi^*$  resonance, but the presence of a  $\sigma^*$  resonance, which occurs at 408 eV. All the four types of fossil-fuel samples show resonances at this energy, which suggests that there may be some amount of saturated amine structures present in them.

Different nitrogen structures show  $\pi^*$  (or  $\sigma^*$ ) resonances at well separated energies, as shown in figure 3. Several analogues of different structures of nitrogen have been studied previously(8,9), and it is found that all analogues belonging to the same structure exhibit  $\pi^*$  resonances at energies close to each other ( $\Delta E \sim 0.5 eV$ ), but well separated from the  $\pi^*$  resonances of the spectra of other structures ( $\Delta E \sim 2 eV$ ). This has been explained by means of the behavior of the lone pair of electrons at the nitrogen site in the molecule. When the electrons are involved in the  $\pi$ -cloud of the six-membered aromatic ring, as in pyrroles and pyridones, the nitrogen site is left slightly positive, and these structures show higher energy  $\pi^*$  resonances. In contrast, in pyridines, the lone pair of electrons are involved in the  $sp^2$  orbital and the nitrogen site is left slightly negative; these structures show lower energy  $\pi^*$  resonances than pyrroles and pyridones.

A least-squares fitting program has been used in order to analyze the coal spectra. All the spectra of models and the coal samples were first normalized with respect to the respective step heights, and were then fit to a sum of several different Lorentzian peaks and an arc-tangent step. The peaks represent bound to bound electronic transitions, and the step represents transition to the continuum. Figure 4(a) shows a typical fitted spectrum of a nitrogen model compound (9-vinylcarbazole), and figure 4(b) shows the fitted spectrum of a coal (PITT). The first seven resonance features of the fossil-fuel spectra were identified to five different types of nitrogen; in order to maintain consistency, all the model and fossil-fuel spectra were fit with the same set of parameters. The relevant peaks were: 399.8 eV,  $\Delta v = 0.8$  eV (pyridine), 401.9 eV,  $\Delta v = 0.97$  eV (pyridone), 402.6 eV,  $\Delta v = 1.3$  eV and 403.7 eV,  $\Delta v = 1.9$  eV (pyrrole), 405.0 eV,

$\Delta v=2.0$  eV (aromatic amine), and 406.2 eV,  $\Delta v=1.4$  eV and 407.9 eV,  $\Delta v=2.9$  eV (all models including saturated amines). A continuum resonance was included to produce better fits to the data but were not used in our analysis procedure; its location was 412.8 eV,  $\Delta v=3.2$  eV. The step was positioned at 408 eV, with a width of 1.5 eV. Average area values of the normalized peaks in the spectra of all analogues belonging to the same nitrogen structure were determined; these values were then used to analyze the coal spectra. For instance, the resonance at 400 eV in the fossil-fuel spectra was attributed to pyridine structure, and the pyridine contribution in the coal spectra was determined; in a likewise manner, other nitrogen contributions were also determined. Care was taken to subtract from the fossil-fuel spectra any secondary contribution arising from a different structure at the same energy as the  $\pi^*$  resonance of the primary structure in consideration. After determining secondary contributions from pyridines, pyridones, and pyrroles at 405 eV, the valley at this energy in the coal spectra was assumed to be "filled in" due to the presence of aromatic amine, and the aromatic amine contribution was determined. The 408 eV resonance was attributed as due to the presence of saturated amines.

Table 1 lists the percentages of the different nitrogen structures present in the coals. All the nitrogen in coals are aromatic in nature, with pyrrolic type being the most dominant. Substantial quantities of pyridinic structures are also found in the high rank coals. The low rank coals have smaller amounts of pyridine and larger amounts of pyridone, as opposed to the high rank coals; this leads to the argument that as coal matures from a low rank stage to a high rank stage, pyridone loses its oxygen and become transformed into pyridine structures. Small quantities of aromatic amine are found in all the coals.

We estimate the errors in the percentages listed in the above tables to be within 12%; there are several sources for such errors. First of all, the ratio of the intensity to the step height of different analogues of the same structure can vary significantly as seen previously, and an average value for the  $\pi^*$  area may introduce some errors. Secondly, the aromatic amine determination is not unique, since the aromatic amine analogues exhibit spectra with broad  $\pi^*$  resonances, and we have assumed that the valley at 405 eV in the fossil-fuel spectra is "filled up" due to the presence of aromatic amine in the fossil-fuel samples. Furthermore, the assignment of peaks in the fossil-fuel spectra to different nitrogen structures is somewhat arbitrary, and a slightly different position would perhaps generate a slightly different set of numbers. However, the trends would remain the same in the percentage values noted above.

## CONCLUSIONS

Five different nitrogen structures have been determined by XANES methodology in several coals of different ranks. Coals have only aromatic nitrogen structures with pyrrolic types being the most dominant. Low rank coals have significant amounts of pyridone and smaller (or no) quantities of pyridine; as these coals mature over geological time to a higher rank stage, the pyridone structures lose their oxygen and become transformed to pyridine types. Aromatic amine is the other form of nitrogen found in these coals. The immature kerogens and bitumens have spectra similar to those of coals, although trends in the intensities of the different resonances among the different kerogen and bitumen spectra are not evident. The peak  $\sim 402$  eV in the bitumen samples may arise from pyridone, as well as some other nitrogen structures; the matter is still under investigation.

- 1) C. E. Spiro, J. Wong, F. W. Lytle, R. B. Greggor, D. Maylotte, and S. Lampson, *Science*, 226, 48 (1984)
- 2) G. P. Huffman, F. E. Huggins, S. Mitra Kirtley, N. Shah, R. Pugmire, B. Davis, F. W. Lytle, and R. B. Greggor, *Energy and Fuels* 3, 200 (1989)
- 3) M. L. Gorbaty, G. N. George, and S. R. Kelemen, *Fuel*, 69, 1065 (1990)
- 4) G. P. Huffman, S. Mitra Kirtley, F. E. Huggins, N. Shah, S. Vaidya, and F. Lu, *Energy and Fuels*, 5, 574 (1991)

- 5) P. Burchill, Intl. Conf. on Coal Science, (J. A. Moulijn, et al Eds.), Elsevier Science Publ. B. V., Amsterdam, (1987)
- 6) P. Burchill, and L. S. Welch, Fuel, 68, 100 (1989)
- 7) S. Mitra-Kirtley, O. C. Mullins, J. van Elp, and S. P. Cramer, Fuel, 72, 133 (1993)
- 8) O. C. Mullins, S. Mitra-Kirtley, J. van Elp, and S. P. Cramer, Appl. Spec., accepted.
- 9) S. Mitra-Kirtley, O. C. Mullins, J. van Elp, S. George, J. Chen, and S. P. Cramer, J. Am. Chem. Soc. 115, 252 (1993)
- 10) C. T. Chen, Nucl. Instrum. Methods Phys. Res., Sect. A 256, 595 (1987); C. T. Chen, and F. Setze, Rev. Sci. Instrum. 60, 1616 (1989)
- 11) S. P. Cramer, O. Tench, M. Yocum, H. Kraner, L. Rogers, V. Radzka, O. C. Mullins, and S. Rescia, X-Ray Absorption Fine Structure - Proc. 6th Intl. XAFS Conf., S. S. Hasnain Ed., Ellis Horwood Chichester, 640 (1991)
- 12) K. S. Vorres, Energy and Fuels, 4(5), 420 (1990)

Table 1. Percentages of different nitrogen structures found in coals of different ranks.

Samples	C	H	O	N	Pyridine	Pyridone	Pyrrrole	Aniline
POC	91.81	4.48	1.66	1.34	18	8	66	8
UF	88.08	4.84	4.72	1.60	18	8	66	8
PITT	84.95	5.43	6.90	1.68	20	8	65	9
WV	85.47	5.44	6.68	1.61	20	16	55	9
UT	81.32	5.81	10.88	1.59	17	15	60	8
L	80.73	5.20	10.11	1.43	20	19	54	7
WY	76.04	5.42	16.90	1.13	10	29	51	10
ND	74.05	4.9	19.13	1.17	2	42	50	6

\* Mass fraction from K. S. Vorres, Users Handbook for the Argonne Premium Coal Sample Program, Argonne National Lab.

# Normalized by nitrogen content

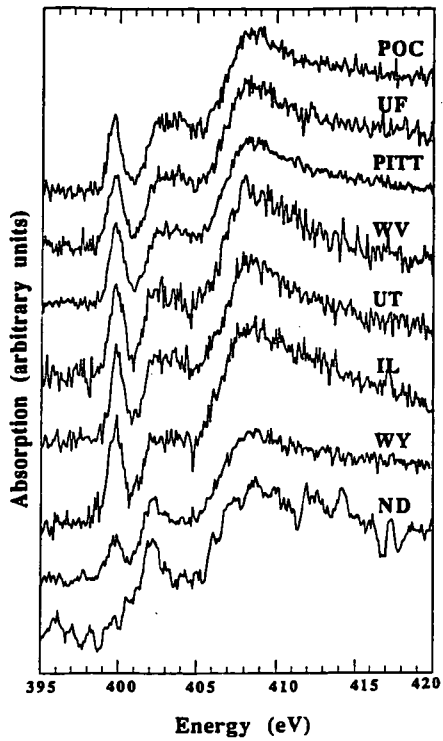


Figure 1. Nitrogen XANES of different coals. The plots are shown in order of coal rank, the higher rank being at the top.

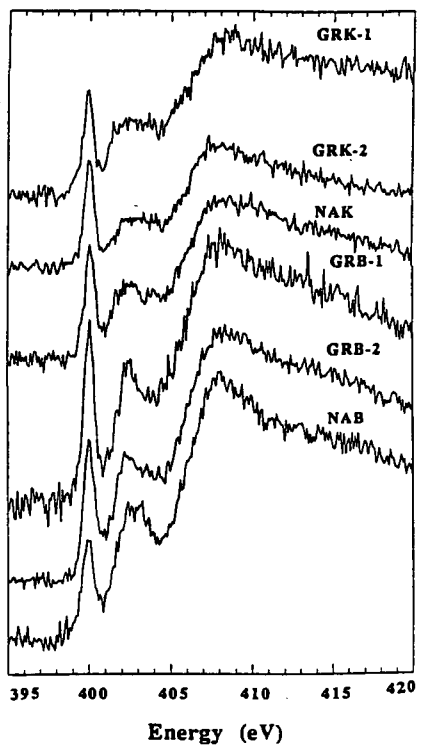


Figure 2. Nitrogen XANES of several kerogens and bitumens.

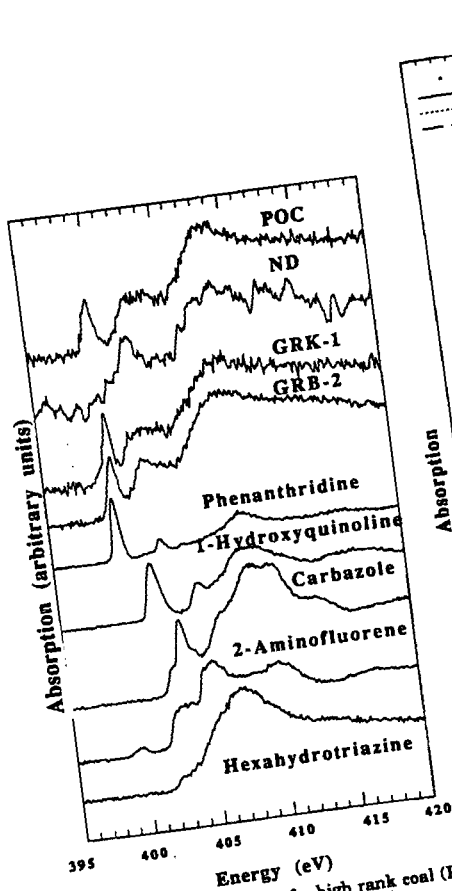


Figure 3. Nitrogen XANES of a high rank coal (POC), a low rank coal (ND), a kerogen (GRK-1), a bitumen (GRB-2), and five different nitrogen structures.

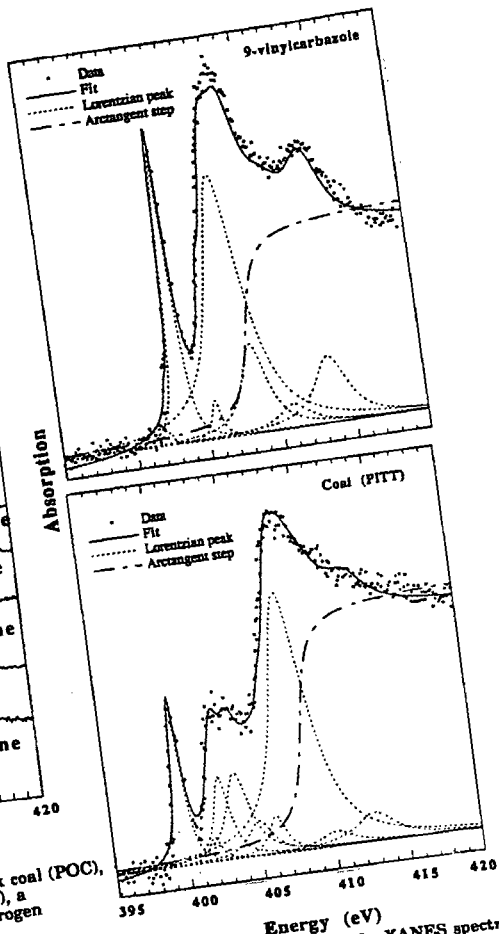


Figure 4. Least squares fit of the XANES spectra of a nitrogen model compound (9-vinylcarbazole) and a coal (PITT).

## **NUMERICAL MODELING OF NITROUS OXIDE FORMATION FROM CHAR COMBUSTION**

**Atsushi Morihara, Claes J. Tullin,  
J. Derek Teare, Adel F. Sarofim and János M. Beér**  
*Department of Chemical Engineering  
and  
Energy Laboratory  
Massachusetts Institute of Technology  
Cambridge, MA 02139*

**Keywords:** coal, nitrous oxide and heterogeneous reaction

### **ABSTRACT**

Growing scientific and public concerns over global warming and ozone layer depletion have led researchers to study the causes for the observed increase in ambient N<sub>2</sub>O concentrations. Man made sources, such as N<sub>2</sub>O emissions from fossil fuel combustion, have been implicated. However, the mechanism for N<sub>2</sub>O formation in coal combustion is not fully understood. It is especially difficult to deal with N<sub>2</sub>O formation since the reactions are complex. In this paper, a model for NO and N<sub>2</sub>O formation and destruction using a single particle model is discussed. The model is based on the experimental observation that the formation of N<sub>2</sub>O is dependent on the existence of both NO and O<sub>2</sub> in the system. Numerical simulations, using the control volume method, show the effects of particle diameter and pressure. The results of the model are compared with experimental data, and show good agreement.

### **INTRODUCTION**

Potential anthropogenic sources of N<sub>2</sub>O that have been investigated include fossil fuel combustion. Until recently, pulverized-coal combustion was implicated as the main source of N<sub>2</sub>O emission due to errors encountered in sampling. It is now known that emissions from these units are typically less than 10 ppm. Fluidized bed combustion (FBC) has emerged as an advanced method of energy production, but for current designs these units have been shown to emit more N<sub>2</sub>O than their pulverized-coal combustion counterparts[1].

In fluidized bed combustion, the emission of N<sub>2</sub>O formed from char decreases with increasing temperature, in contrast to the trend for char NO emissions that increase or pass through a maximum with increasing temperature[2][3]. The char nitrogen conversion to NO as a function of temperature has been determined by Yue using an analytical solution[4]. Yue's approach is based on first order kinetics. The complex N<sub>2</sub>O reactions, however,

preclude an analytical solution, and a numerical approach is indispensable for calculating the fraction of the char nitrogen converted to N<sub>2</sub>O.

The mechanism used in this paper is an extension of that developed by de Soete[5] in which it is postulated that (-CN) reacts with O<sub>2</sub> to form (-CNO) and the (-CNO) next reacts with NO to form N<sub>2</sub>O. The (-CNO) can also dissociate to form NO.

### FUNDAMENTAL EQUATIONS

The fundamental reactions leading to NO and N<sub>2</sub>O formation and destruction are considered to be:



NO and N<sub>2</sub>O are mainly reduced heterogeneously by carbon. The formation reaction rates of NO  $r_{NO}$  and that of N<sub>2</sub>O  $r_{N_2O}$  are given by:

$$r_{NO} = k_2 [(-CNO)] \quad (6)$$

$$r_{N_2O} = k_3 [NO] \cdot [(-CNO)] \quad (7)$$

The fractions of char-nitrogen transformed into NO and N<sub>2</sub>O has been shown to be roughly proportional to the fraction of carbon burnt[4]. The total nitrogen oxidation rate,  $f_N$ , is therefore equal to the product of N/C ratio and reaction rate of carbon oxidation,  $f_C$ :

$$f_N = r_{NO} + 2 \cdot r_{N_2O} = \frac{N}{C} f_C \quad (8)$$

$f_C$  in turn is calculated using reaction rate information from Smith[6]. By manipulating Eqs.(6), (7), and (8), the concentration of (-CNO) can be shown to be:

$$[(-CNO)] = \frac{\frac{N}{C} f_C}{k_2 + 2 \cdot k_3 [NO]} \quad (9)$$

If we replace (-CNO) in Eqs.(6) and (7) by Eq.(9), the reaction rates of NO and N<sub>2</sub>O are given by:

$$r_{NO} = \frac{N}{C} f_c \cdot (1 - 2\alpha) \quad (10)$$

$$r_{N_2O} = \frac{N}{C} f_c \cdot \alpha \quad (11)$$

where

$$\alpha = \frac{k_3[NO]}{k_2} \left( 1 + 2 \cdot \frac{k_3[NO]}{k_2} \right)^{-1} \quad (12)$$

If the NO concentration is small enough, Eqs.(10) and (11) become:

$$r_{NO} = \frac{N}{C} f_c \cdot (1 - 2 \cdot k_r[NO]) \quad (13)$$

$$r_{N_2O} = \frac{N}{C} f_c \cdot k_r[NO] \quad (14)$$

$$k_r = k_3 / k_2 \quad (15)$$

$k_r$  is a function only of temperature. If the reaction rate of carbon oxidization is proportional to O<sub>2</sub> concentration, then the rate of conversion of nitrogen in the char to N<sub>2</sub>O is proportional to the NO and O<sub>2</sub> concentrations, and the rest of the nitrogen in the char is converted to NO.

## CALCULATION

A material balance on a spherical shell in the carbon particle yields:

$$De_i \frac{1}{r^2} \left( r^2 \frac{\partial}{\partial r} C_i \right) + f_i(C_1, C_2, \dots) = 0 \quad (16)$$

where  $C_i$  is the concentration of the  $i$  th species, where  $i$  can be O<sub>2</sub>, CO, CO<sub>2</sub>, NO, and N<sub>2</sub>O.  $De_i$  represents the effective diffusivity of component  $i$  calculated on the basis of Knudsen diffusion within the pores of the char particle.  $r$  is radial distance from the center of the particle.  $f_i(C_1, C_2, \dots)$  is the reaction term. The boundary conditions are given by:

$$-De_i \frac{\partial C_i}{\partial r} \Big|_{r=R_p} = k_m (C_i|_{r=R_p} - C_i|_{r \rightarrow \infty}) \quad (17)$$

where  $k_m$  is the external mass transfer coefficient and  $R_p$  is the particle radius[7][8].

Figure 1 shows the calculation cell of the particle, which is a portion of the spherical shell. To allow for the concentration of the reaction near the particle surface, the shell thickness decreases with increasing radius. The destruction and formation reactions are assumed to be uniformly distributed in a cell volume, and

diffusion between cells is formulated at each cell surface. For the exterior cell the diffusion to the surface is equated to the external mass transfer.

An example of a typical concentration profile is shown on the same figure. O<sub>2</sub> is consumed near the surface of the particle. NO is also formed in this region, and it either diffuses towards the center of the particle where it reacts with the char or it diffuses to the surface where it escapes from the particle. As a result, the NO concentration in the particle is depleted at the center of the particle where the NO consumption reactions prevail, increases to a maximum nearer the surface where the NO is produced, and falls at the surface due to the NO diffusion out of the particle. N<sub>2</sub>O is formed at the same time as NO at a rate proportional to the local NO concentration. Part of the N<sub>2</sub>O is also destroyed in the particle by reaction with carbon. Because the N<sub>2</sub>O destruction rate is low the N<sub>2</sub>O concentration can increase with decreasing radius.

## EXPERIMENTAL

Batch combustion experiments were performed in a small scale quartz glass bubbling fluidized bed reactor (inner diameter 57 mm). A bed of Silica sand (particle size 150-212 μm), with a bed height of approximately 50 mm, was fluidized by a mixture 8 % O<sub>2</sub> in helium. The composition and flow rate were controlled using mass flow controllers. The flow rate was set to 2.5 l/min NTP (273 K 1 atm). In each experiment, coal particles (diameter 4 mm) were burned. The concentrations of the combustion products, N<sub>2</sub>O, NO, O<sub>2</sub>, CO<sub>2</sub>, CO, and CH<sub>4</sub>, were obtained using a FTIR spectrometer equipped with a MCT detector, and a low volume (223 cm<sup>2</sup>) gas cell with variable path length, which was set to 7.25 m in the experiments discussed here. A detailed description of the reactor and experimental set-up can be found elsewhere[9].

The fractions of char nitrogen converted to NO and N<sub>2</sub>O as functions of carbon conversion can be calculated from the concentrations and gas flow rate. The instantaneous conversions to NO and N<sub>2</sub>O are given by:

$$f_{N_2O} = \frac{2[N_2O]}{\frac{N}{C} \sum([CO_2] + [CO] + [CH_4])} \quad (18)$$

$$f_{NO} = \frac{[NO]}{\frac{N}{C} \sum([CO_2] + [CO] + [CH_4])} \quad (19)$$

## COMPARISON

The effect of particle radius on the fraction of fuel nitrogen converted to NO and N<sub>2</sub>O is shown in Figure 2. These calculations were performed by assuming a shrinking particle model. The calculated conversions to NO and N<sub>2</sub>O, which are functions of the shrinking sphere radius, are compared with the data. The conversion to NO decreases with increasing radius, while the conversion to N<sub>2</sub>O

increases. The calculated results show the formation and destruction of both NO and N<sub>2</sub>O. The ratio of N<sub>2</sub>O formation rate to total rate increases with increasing radius, since the NO concentration in the pore increases with increasing radius.

With the model in this way effectively validated by comparison with data at atmospheric pressure, it is reasonable to use it for prediction of behavior at higher pressures. For example, one can calculate the effect of decrease in the external mass transfer coefficient due to increase in pressure. The effect of this is shown in Figure 3. The conversions of the fuel nitrogen to NO and N<sub>2</sub>O can be shown, from consideration of the governing equations, to be functions of four dimensionless groups: three Thiele moduli  $R_p\sqrt{k_{O_2}/D_e}$ ,  $R_p\sqrt{k_{NO}/D_e}$ ,  $R_p\sqrt{k_{N_2O}/D_e}$ , and the Biot number  $k_m R_p/D_e$ , where  $k_{O_2}$ ,  $k_{NO}$ , and  $k_{N_2O}$  are the rate constants for the reactions of O<sub>2</sub>, NO, and N<sub>2</sub>O with char,  $k_m$  is the external mass transfer coefficient, and  $D_e$  the effective diffusivity in the pores of the particle. Only  $k_m$  is a function of pressure since it is directly proportional to the bulk gas diffusivity, which in turn is inversely proportional to pressure. The model can therefore be used to predict the effect of pressure by varying the Biot number. These results, for representative values of the Thiele moduli, are shown in Figure 3. The predicted results show that NO decreases with increased pressure, consistent with the limited available measurements.

Thus the model, based on comparatively simple formation and destruction mechanisms, yields good agreement between experimental data and the calculation results.

## CONCLUSION

For the conditions studied (a Newland, Australia bituminous coal) as the char conversion increases, the conversion of char nitrogen to NO increases, approaching one in the limit, while that to N<sub>2</sub>O decreases with decreasing radius.

The results can be well modeled by assuming that, as the char is oxidized, the associated char nitrogen is converted to either N<sub>2</sub>O or NO, with the split depending on the local NO concentration, and that there is a subsequent partial reduction of the NO and N<sub>2</sub>O as these species diffuse through the porous char to the particle surface.

## REFERENCES

1. M. D. Mann, M. D. Collings, and E. B. Botros "Nitrous Oxide Emissions in Fluidized-bed Combustion: Fundamental Chemistry and Combustion Testing." *Prog. Energy Combust. Sci.* 1992, Vol.18, pp. 447-461
2. Atsushi Morihara, Claes J. Tullin, Adel F. Sarofim and János M. Beér "Oxidization of Char Nitrogen: Extrapolation of Results from Fluidized Bed Reactors to Pulverized Coal Flames" 7th Topic Oriented Technical Meeting, May 1993

3. Claes J. Tullin, Adel F. Sarofim and János M. Beér "NO and N<sub>2</sub>O Formation for Coal Combustion in a Fluidized Bed: Effect of Carbon Conversion and Bed Temperature" (Submitted to Energy & Fuel, April 1993)
4. G. X. Yue, F. J. Pereira, Adel F. Sarofim and Janós M. Beér, "Char Nitrogen Conversion to NO<sub>x</sub> in Fluidized Bed", Combustion Science and Technology, 1992. Vol. 83, pp. 245-256
5. G. G. de Soete "Heterogeneous N<sub>2</sub>O and NO Formation from Bound Nitrogen Atoms during Coal Char Combustion" Twenty-Third Symposium (International) on Combustion, 1990, pp. 1257-1264
6. I. W. Smith "The Combustion Rates of Coal Chars: A review" Ninth Symposium (International) on Combustion Institute, 1982, pp. 1045-1065
7. Octave Levenspiel "Chemical Reaction Engineering" Second Edition, John Wiley & Sons, Inc. pp. 357-401, 1972
9. Claes J. Tullin, Adel F. Sarofim and János M. Beér "Formation of NO and N<sub>2</sub>O in Coal Combustion: The Relative Importance of Volatile and Char Nitrogen" 12 th International Conference on Fluidized Bed Combustion, pp. 599-609, May 1993

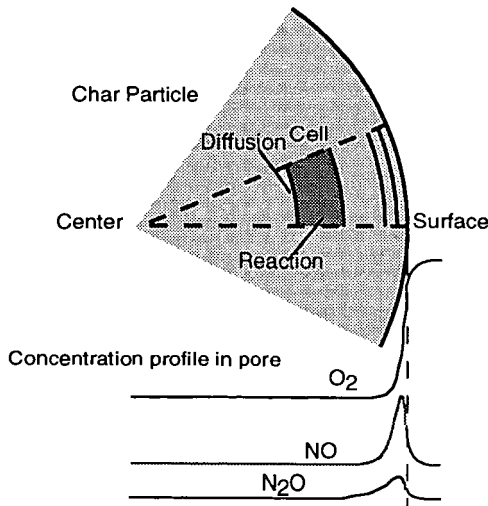


Figure 1 Calculation method and concentration profiles in the particle

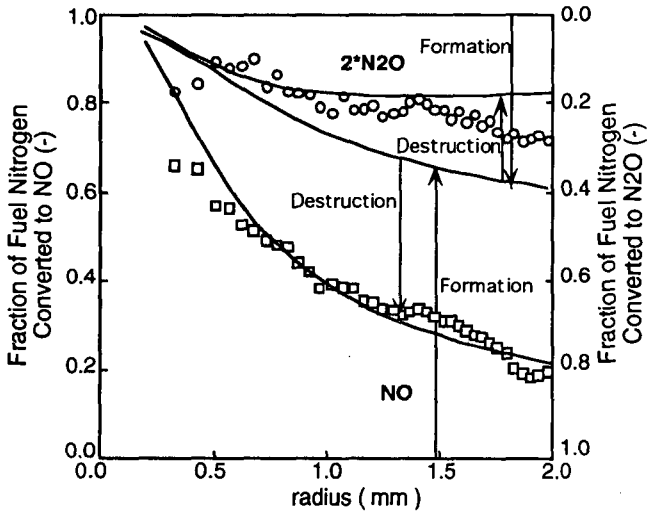


Figure 2 Effect of particle radius on char nitrogen conversion rate to NO and N<sub>2</sub>O

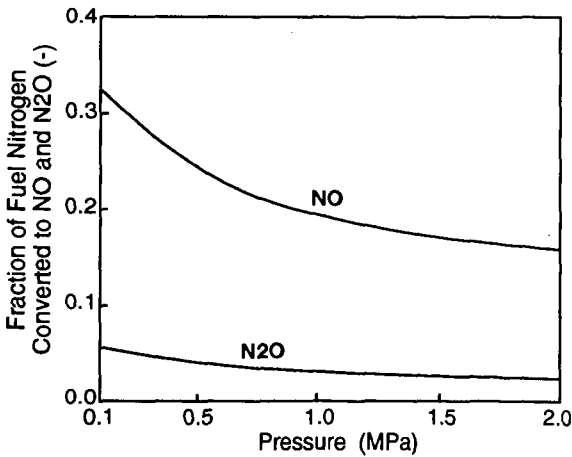


Figure 3 Effect of pressure on char nitrogen conversion rate to NO and N<sub>2</sub>O

## Effect of Unleaded Fuel on Octane Requirements of Automobile Engines

R G Temple, Department of Chemical Engineering & Applied Chemistry, Aston University, Aston Triangle, Birmingham B4 7ET, UK.

J Ahmed, Energy Technology Support Unit, Harwell, Oxfordshire OX11 0RA, UK.

Unleaded fuels are increasingly supplanting lead-treated fuels throughout the world. Initiatives in the USA, in Europe and in many industrialised countries are leading to social and legislative constraints against the use of lead compounds as additives. Alternative gasoline formulations are being developed to restore the octane rating, which for more than fifty years has been boosted by lead. Initially, increased proportions of aromatics were included in the gasoline fraction, but these also have undesirable environmental consequences and substitute oxygenates (alcohols, ketones and ethers) are proving to be excellent octane boosters.

Apart from their octane rating benefits, the use of lead compounds has other consequences. Like certain other metals, lead provides some lubricant properties, eg with inlet and exhaust valve operation. Continuous provision of a miniscule layer of lead on metallic surfaces inside the combustion chamber proved inadvertently to be highly effective as a lubricant for adjacent surfaces sliding against each other at the very high frequency required. Using lead-free fuels may in the long-term alter the life of inlet and exhaust valves and valve stems and other engine components but no great concern on this matter has yet been heard. However a notable feature of the use of lead-free fuel is the progressive increase of octane requirement. Initially, ie, with a new engine, or with "clean"

reconditioned surfaces, octane number is determined by the fuel formulation. Then with lead-free fuel a small but steady increase in octane requirement is noted. This has been attributed to the changed nature of combustion chamber deposits compared with the deposits from leaded fuels.

Combustion chamber deposits may affect octane requirements in three ways:

- 1 ) by occupying physical volume
- 2 ) by surface activity catalysing (or inhibiting) combustion reactions
- 3 ) by heat transfer effects due to changed thermal conductivity.

In our work at Aston we were most concerned with the physical properties of deposits studying the nature of the solid layers with scanning electron microscope to establish comparisons of porosity. Measurement of thermal conductivity was also undertaken since deposit surface temperature is almost certainly a key factor in knock-related reactions which determine octane requirements.

### The nature of combustion chamber deposits

High boiling point hydrocarbons condense on the cooled walls and are partly burned off leaving a carbonaceous layer. With leaded fuels a layer of condensed lead compounds will cover and mingle with the carbonaceous layer. Lead oxide initially deposited will form lead salts - halides and sulphates. At low

temperatures, halides are favoured. As the engine warms up only the highest boiling hydrocarbons condense, leading to less carbonaceous material but the lead salts continue to build up, progressively increasing the deposit thickness. The deposit reduces heat transfer to the cooling water leading to increased deposit surface temperature. At this higher temperature lead sulphate formation is favoured.

#### Deposit removal

Volatilisation effects, which lead to some removal of deposit material, depends on engine operating conditions, higher chamber temperatures leading to greater deposit removal. Changes in chemical composition of deposits were similar to changes resulting from higher wall temperatures suggesting that the insulating effect of the deposit causes significant surface temperature increase as the deposit builds up.

Since engines are commonly run intermittently deposits will be formed in layers so that the deposit presents a stratified structure. Changes in chemical nature of the deposit would be expected as the total deposit layer increases in thickness.

As the deposit layer increases, internal temperature gradients will be set up and are likely to lead to flaking. Any mechanical or thermal shock will accelerate flake detachment. Flecking, or the detachment of small flakes, is also recognised on very thin deposit layers.

#### Deposit Adhesion

Adhesion of the deposit layers is partly chemical in nature. At higher temperatures the

carbonaceous material will be oxidised forming a link between deposit and wall metal and then between successive deposit layers.

#### Deposits from Leaded Fuel

The introduction of lead into fuel is reported to lead to a four-fold increase in deposit weight. Dumont<sup>(1)</sup> showed that 25% of the resulting ORI (octane requirement increase) was due to volume effect and remainder to the insulating effect.

The carbonaceous portion of the deposit also depends on the type of crank-case oil and the amount of oil reaching the combustion chamber surfaces. Synthetic (polymer) lube-oils gave lower ORI values than conventional lube oils. However C<sup>14</sup> tracer experiments have indicated that the fuel is responsible for 70% of the deposit.

#### Comparison of thermal conductivity

In our work we assessed thermal conductivities in a method designed to simulate *in situ* conditions. Every attempt was made to avoid disturbance of deposit with partial destruction of the porous structure. Heat Flow from a copper bar of larger radius than the piston was monitored as shown in fig 1. It was impracticable to ensure a completely flat contact surface owing to the irregular nature of the deposit surface.

The lower end of the copper bar was drilled to house four 0.75 kW cartridge heaters. Variable voltage input enabled several steady state readings to be obtained for calculation of effective thermal conductivity.

### Assessment of permeability and porosity

These properties are important in relation to ORI since a porous deposit may trap residual combustible mixture enabling this to initiate subsequent precombustion reactions. It is also likely to trap exhaust gases discharging heat to the fresh incoming charge. Both phenomena are likely to contribute to ORI.

Permeability and porosity were measured using standard Lea & Nurse apparatus (fig 2).

### Experimental Results

Lead-free fuel deposit was obtained on a car using US fuel over 1300 km of average operating conditions for a private passenger car. The leaded fuel deposit was from a similar engine in UK over 1480 km.

Thermal conductivity of the leaded-fuel deposit was  $0.75 \text{ Wm}^{-1}\text{K}^{-1}$  while the lead-free fuel deposit showed a value of  $0.5 \text{ Wm}^{-1}\text{K}^{-1}$ . This lower thermal conductivity will naturally lead to higher surface temperature and increased tendency to induce knock. Furthermore the result of introduction of lead free fuel will be a progressive increase in octane requirement as the deposit builds up on piston head and combustion chamber walls, etc.

Volumetric effect of the deposit was also assessed. It is obvious that even a small change in deposit thickness alters compression ratio significantly. With a possible increase of compression ratio of around 0.25 units, lead-free deposits may well lead to an increased requirement of two octane numbers. Many researchers have reported deposits of much greater thickness.

Permeability and porosity effects are more difficult to quantify. The diffusion of reacting combustion chamber gases into the porous structure of the deposit will affect the influence of the nature of the solid surface on knock-inducing reactions and the relative areas of such surfaces available for contact with the gases. The lead-free deposit was shown microscopically to consist of a two-layer stratum, the outer layer more porous than the inner. Owing to this structure and the size of sample available it was not possible to make a meaningful comparison of deposit permeability.

The chemical nature of the deposits were compared by scanning electron microscope but it is impossible to make quantitative comparisons from the contrasting analyses. Mineral constituents (barium, aluminium and zinc, etc) prominent in the lead-free deposit, presumably arise from processing catalyst residues.

The two-layer structure of the lead-free deposit is clearly visible but otherwise scanning electron microscope photographs merely confirm the contrasting porosity and grain structure of the deposits.

### Conclusions

Quantitative conclusions are difficult because of diverse factors affecting engine combustion conditions. Driving behaviour, patterns of use, driving cycle, comparisons of acceleration, high-speed running and idling modes show wide variation across metropolitan, urban, and cross-country areas. These variations and engine size and load variations make precise prediction almost impossible.

However our work has confirmed that deposits from lead-free fuel do throw some light on the octane requirement increase resulting from the elimination of lead.

Further changes may now be expected as new unleaded fuel formulations replace the first generation of lead free fuels. The replacement of aromatics by oxygenates as octane improvers could well have a significant effect on deposit quality, quantity, and volume.

#### Reference

- (1) Milkita J.J. and Sturgis, B.B. The Chemistry of Combustion Chamber Deposits. S.A.E. Journal 1957 65.

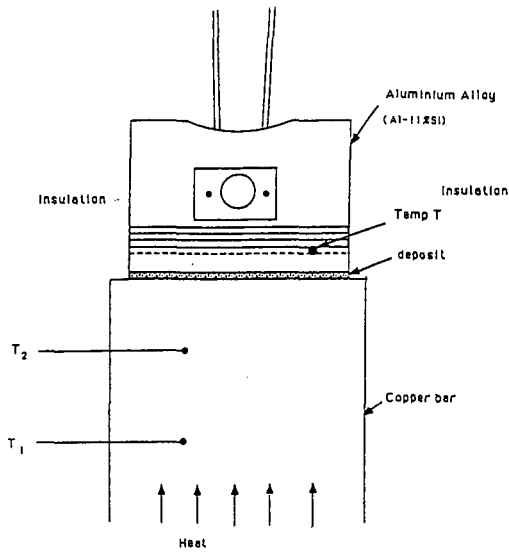
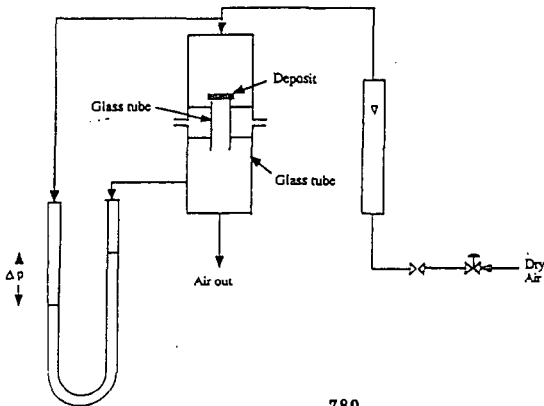


Figure 1. Measurement of Thermal Conductivity

Figure 2. Diagrammatic Presentation of Permeability Apparatus



## CHARACTERIZATION AND DEPOSIT FORMING-TENDENCY OF POLAR COMPOUNDS IN CRACKED COMPONENTS OF GASOLINE. IDENTIFICATION OF OXIDIZED SULFUR COMPOUNDS.

Pedro Martín, Lola De Lima and Anibal Rojas\*

Centro de Investigación y Apoyo Tecnológico INTEVEP s.a., Filial de PDVSA, Apartado 76343, Caracas 1070A, VENEZUELA.

\*Escuela de Química, Facultad de Ciencias, Universidad Central de Venezuela, Apartado 47102, Los Chaguaramos, Caracas, VENEZUELA.

Keywords: FCC composition, ISD Deposit formation, Oxidized benzothiophenes

### ABSTRACT

In order to evaluate the deposit forming-tendency of polar compounds in gasoline, one FCC component from a Venezuelan refinery was studied. The polar compounds were separated by column chromatography on alumina, using hexane, benzene, ethyl acetate and methanol as eluents, and their deposit forming-tendencies were determined by ISD apparatus. The ethyl acetate and methanol fractions showed high tendencies to form deposits. Identification of the different components of these fractions was intended by spectroscopic methods (IR,  $^1\text{H}$  and  $^{13}\text{C}$ -NMR and GC-MS) in subfractions obtained by further column and thin layer chromatographies. The main components were identified as mono- and dimethyl 2,3-dihydrobenzothiophene-S,S-dioxides in the ethyl acetate fraction, and mono- and dimethyl benzothiophene-S-oxides in the methanol fraction. This is the first report on the presence of this type of compound in gasoline components, and on their role as deposit-forming promoter.

### INTRODUCTION

The role of oxidized compounds in deposit formation in the induction system of gasoline engines has been reported. This type of compounds have a natural affinity for metal surfaces and may react vigorously on the surface forming high deposit levels. Taniguchi (1) found that polar materials are implicated in Port Fuel Injector (PFI) deposit formation. Laboratory test showed that deposit formation was reduced when polar compounds were removed from unstable gasolines (2). Alcohol and catalytic cracked components in the fuel have been found to increase inlet valve deposits (3). The thermal decomposition of oxidized polar compounds, such as ketones, alcohols, carboxylic acids and others, contained in the fuel or formed by oxidation of fuel olefins increased of the ISD deposit formation (4).

This study reports the characterization of two sulfur-rich and high polar fractions obtained by adsorption chromatography a cracked gasoline component and their contributions to deposit formation.

### EXPERIMENTAL

#### Separation

The cracked gasoline component FCC-1 was subjected to acid-base extraction and adsorption chromatography on a column packed with neutral aluminum oxide, according to a previously described procedure (5). The material retained on the column was eluted with one gallon each of the following solvents: hexane, benzene, ethyl acetate and methanol. These fractions were evaporated under reduced pressure ( $T < 50^\circ\text{C}$ ) under an inert atmosphere.

#### Instrumentation

The carbon-13 and hydrogen-1 NMR spectra were recorded with a Bruker MSL-300 or an ACP-400 spectrometer at room temperature, using  $\text{CDCl}_3$  as solvent and TMS as internal standard. Samples were contained in 5 mm i.d. nmr cells.

The mass spectra of the ethyl acetate fraction was obtained with a Hewlett Packard 5995A GC/MS apparatus, equipped with a 60 m x 0.32 mm i.d. (0.25  $\mu\text{m}$  film) DB-1 Megabore column, programmed from 50-200 $^\circ\text{C}$  at 5 $^\circ\text{C}/\text{min}$ , using helium as carrier gas. The GC/MS of the methanol fraction was obtained with a Ruska Laboratories apparatus, equipped with a 30 m x 0.32 mm i.d (0.25  $\mu\text{m}$  film) DB-5 column with the same temperature program.

Infrared spectra were recorded with a Perkin-Elmer model 1310. The samples were prepared as thin films on NaCl plates.

Total nitrogen and sulfur contents were determined by chemiluminescence and x-ray (ASTM D-2622) methods.

The subfraction R-1-D was analyzed by GC using a Hewlett Packard 5890A apparatus equipped with a sulfur-selective chemiluminescence detector (Sievers 350B), under similar chromatographic conditions as those used for the GC/MS analyses.

In order to evaluate the deposit-forming tendency of the isolated fractions, 1000 ppm solutions of each fraction in the original FCC-1 sample were tested in an Induction System Deposit (ISD) apparatus (6). This apparatus simulates intake valve deposit formation. Fuels with a high deposit-forming tendency produce > 2 mg/100ml fuel.

## RESULTS AND DISCUSSION

### Ethyl acetate fraction.

The elemental analyses of the ethyl acetate fraction showed a high level of sulfur (2.9%) and a low level of nitrogen (0.2%). The ISD evaluation showed a high deposit-forming tendency (2.8 mg/100ml).

The IR spectrum of this fraction showed bands at 3600-3400, 2900-2800, 1750-1650 y 1150-1050  $\text{cm}^{-1}$ , assignable to O-Hst, C-Hst (alifatic), C=Ost y C-Ost, respectively.

The  $^1\text{H-NMR}$  spectrum showed strong signals at 8-7 ppm (ArC-H), 2-2.6 ppm (Ar-CH<sub>3</sub> and/or H of saturate cycles) and 1.5-0.8 ppm -(CH<sub>2</sub>)- and lower intensity signals at 5-6 ppm =C-H, 3-3.5 ppm -CH-X (X=O or N or S=O) and/or -CH<sub>2</sub>-C=O.

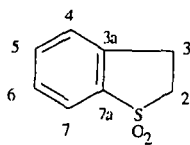
The  $^{13}\text{C-NMR}$  showed very different kind of signals. The more important were located at 120-142 ppm (ArC and/or =C-H), 200-210 ppm (R-C=O, R-O-C=O and/or H-C=O), 172-170 ppm (HO-C=O), 62-64 ppm (HO-CH<sub>2</sub> and/or R-O-CH<sub>2</sub>-), 50-55 ppm (-CH<sub>2</sub>-C=O in saturated cycles, -O-CH<sub>3</sub> or -CH<sub>2</sub>-S=O<sub>x</sub>), 40-48 ppm (-CH<sub>2</sub>- y -CH saturates cycles) and 10-30 ppm (-CH<sub>2</sub>)<sub>x</sub> and/or Ar-CH<sub>3</sub>.

This fraction was subjected to adsorption chromatographic on a column packed with silica gel. The material retained on the column was eluted with mixtures of benzene, benzene-chloroform and chloroform-methanol, obtaining three fractions: R-1-A (7.7%), R-1-B (17.8%) and R-1-D (74.5%).

The subfractions R-1-A and R-1-B were identified as mixture of dimethylnaphthalenes and phthalic acid derivatives, respectively.

The carbon-13 NMR spectrum (Fig.1) of the major fraction R-1-D showed strong signals in the 50-53 ppm zone, assignable to -CH<sub>2</sub>-C=O of saturated cycles, -O-CH<sub>3</sub> or -CH<sub>n</sub>-S=O<sub>x</sub> (n=1,2 and x=1,2). A DEPT experiment showed that these signals corresponded to -CH<sub>2</sub>- groups. The GC analysis of this subfraction with a sulfur-selective detector showed the presence of sulfur compounds.

A detailed study of the carbon-13 NMR chemical shift data of this subfraction indicated the presence of 2,3-dihydrobenzothiophene, S,S-dioxide (7):



CARBON N°	OBSERVED $\delta$ (ppm)	REPORTED $\delta$ (ppm)
2	50.6	50.6
3	25.4	25.3
4	128.7	128.8
5	133.4	133.4
6	127.3	127.2
7	121.3	121.5
3a	137.2	137.2
7a	138.9	138.9

The GC/MS chromatogram (Fig.2) showed ten strong signals. Only one of these peaks was identified as 2,3-dihydrobenzothiophene, S,S-dioxide (m/e 168) according to the NIST Library mass spectral data (N° 12353) and in agreement with our  $^{13}\text{C-NMR}$  results. The  $M^+$  of the other signals: 182 (168+14) and 196 (168+14+14) suggested the presence of methyl- and dimethyl- 2,3-dihydrobenzothiophene, S,S-dioxide. Figures 3 and 4 show probable fragmentation ways of these compounds. Other compounds were identified as methyl and dimethyl indanones, present in minor concentrations.

### Methanol fraction.

The elemental analyses of the methanol fraction showed the highest level of sulfur (3.5%) of all the obtained fractions and a low level of nitrogen (0.2%). The ISD evaluation showed also the highest deposit-forming tendency (6.1 mg/100ml).

The IR spectrum of methanol fraction showed bands at 3600-3400, 2980-2880, 1750-1650 and 1150-1050  $\text{cm}^{-1}$

assignable to O-Hst, C-Hst (alifatic), C=Ost and C-Ost or S=Ost, respectively.

The hydrogen-1 NMR spectrum showed strong signals at 8-7 ppm (ArC-H), 2-2,6 ppm (Ar-CH<sub>3</sub> and/or H of saturated cycles) and 1,8-1,0 ppm (-CH<sub>2</sub>)<sub>x</sub>-, and lower intensity signals at 5-6 ppm (=C-H) and 3-4 ppm (-CH-X X=O or N or S=O and/or -CH<sub>2</sub>-C=O).

The carbon-13 NMR spectrum showed many different types of signals. The more important were located at 115-158 ppm (ArC and/or -C=C-H), 200-210 ppm (R-C=O), 173,6 ppm (HO-C=O or RO-C=O), 76-64 ppm (-CH-OH), 50-53 ppm (-CH<sub>2</sub>-C=O in saturated cycles and/or O-CH<sub>3</sub>), and 12,7-20,9 ppm (-CH<sub>2</sub>- and/or Ar-CH<sub>3</sub>).

This fraction was subjected to adsorption chromatography on a column packed with silica gel. The material retained on the column was eluted with mixtures of chloroform-methanol, obtained one major fraction R-2-B (73.3%).

The IR spectrum of this fraction showed a strong band located at 1060-1020 cm<sup>-1</sup> attribute to S=Ost in sulfones. A detailed study of the carbon-13 NMR chemical shift data of this subfraction indicated the presence of 1- and 2-methyl benzothiophene, S-oxide and 1,2-dimethyl benzothiophene, S-oxide (Table 1).

The GC/MS analysis indicated 1- and 2-methyl benzothiophene, S-oxide (m/c 164), confirming the previous carbon-13 NMR assignments (8). The M<sup>+</sup> of the others signals: 178 (164+14) suggested the presence of dimethyl benzothiophene, S-oxide. Fig. 5 show probable fragmentation ways for these compounds. Other compounds, present in minor concentrations, were identified as benzothiophene, methyl- and dimethyl-benzothiophenes.

To our knowledge, this is the first report demonstrating the presence of this type of compounds in gasoline fractions, and revealing the importance as promoter in the formation of deposit..

#### ACKNOWLEDGEMENT

The authors thank the Internal Market Coordination of Petróleos de Venezuela, S.A. (PDVSA) for financial support, Julio Medina and Ursula Ehrmann of Analisis and Evaluation Section of INTEVEP for the GC/MS spectra, Guillermo Rodriguez, head of the Fuels Section of INTEVEP for his support and comments on this work.

#### REFERENCES

- 1.- Taniguchi B., Peyla R., Parsons G., Hoekman S. and Voss D.: "Injector Deposits-The Tip of Intake System Deposit Problems.", *SAE Paper* N° 861534, 1986.
- 2.- Kim C., Tseregounis S. and Scruggs B.: "Deposit Formation on a Metal Surface in Oxidised gasolines.", *SAE Paper* N° 872112, 1987.
- 3.- Bitting W., Gschwendner F., Kohlepp W., Kothe M., Testvoet C. and Ziwicki K.: "Intake Valve Deposit-Fuel Detergency requirements revisited.", *SAE Paper* N° 872117, 1987.
- 4.- Martín P., McCarty, F. and Bustamante D.: "Mechanism of Deposit Formation: Deposit Tendency of Cracked Components by Boiling Range.", *SAE Paper* N° 922217, 1992.
- 5.- Martín P., McCarty, F., Ehrmann, U., De Lima, L. and Rojas A.: "Characterization and Deposit-Forming Tendency of Polar Compounds in Cracked Components of Gasoline. General Scheme and Identification of Basic Fractions.", *Fuel Science and Technology Int.*, 1993, in press.
- 6.- Dimitroff E. and Johnston A.: "A Bench Technique for Evaluating the Induction System Deposit Tendencies of Motor Gasolines.", *Sae Paper* No 660783, 1966.
- 7.- Genete P., Olivé J., Ung S., Faghi M., Easton J., Beierbeck H. and Saunders J.: "Carbon-13 Nuclear Magnetic Resonance Study of Benzothiophenes and Benzothiophene S-Oxides and S,S-Dioxides.", *J. Org. Chem.*, 44(16), 2887-2892, 1979.
- 8.- Genete P., Grimaud J., Olivé L. and Ung N.: "Oxidation en Sulfoxydes de Benzothiophenes monosubstitues.", *Bulletin de la Société Chimique de France*, (3-4), 255-276, 1977.

Table 1. Carbon-13 NMR chemical shifts of subfractions R-2-B fraction (Observed vs. Reported<sup>(7)</sup> values).

Carbon	Reported	Observed
2	150.6	149.8
3	128.7	128.7
4	127.6	127.5
5	132.0	131.9
6	123.7	123.7
7	126.1	126.0
3a	138.2	138.0
7a	144.8	145.2
2-Me	12.8	12.8

Carbon	Reported	Observed
2	132.1	132.0
3	145.2	145.2
4	128.7	128.9
5	131.8	131.6
6	122.5	122.6
7	125.8	125.8
3a	138.5	138.3
7a	145.9	145.5
3-Me	14.1	14.0

Carbon	Reported	Observed
2	143.7	143.9
3	136.5	136.7
4	127.6	127.5
5	131.9	131.9
6	121.6	121.6
7	125.7	125.5
3a	139.9	139.8
7a	142.9	143.0
2-Me	10.6	10.4

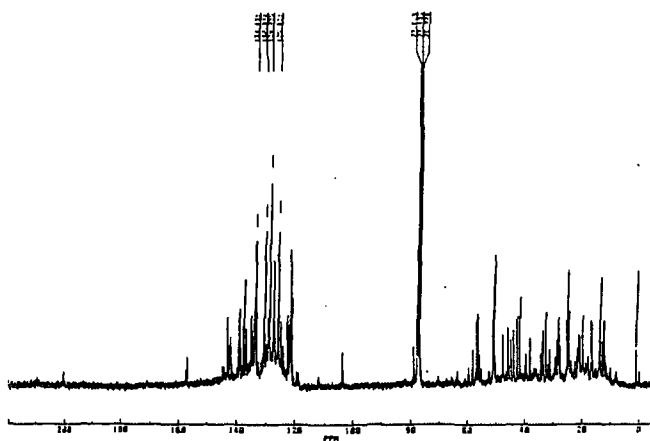


Fig.1 Carbon-13 NMR spectrum of fraction R-1-D.

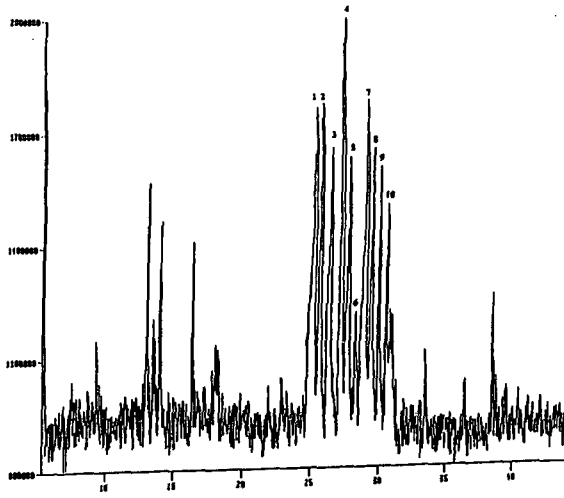


Fig.2 GC/MS chromatogram of fraction R-1-D.

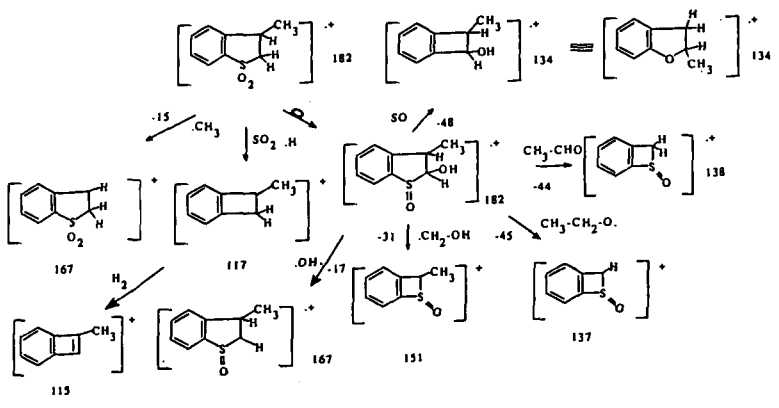


Fig.3 Probable mass fragmentation of methyl-2,3-dihydrobenzothiophene, S,S-dioxide.

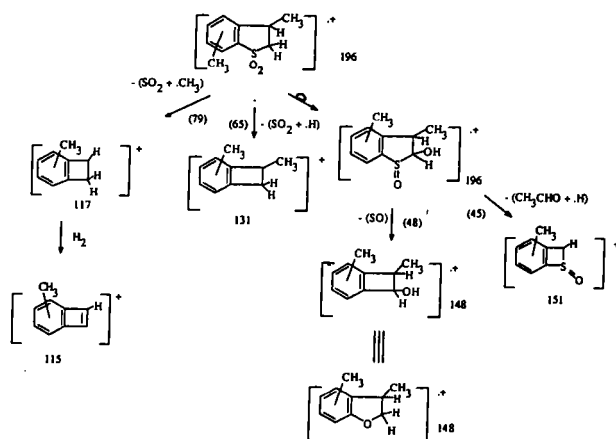


Fig.4 Probable mass fragmentation of dimethyl-2,3-dihydrobenzothiophene, S,S-dioxide.

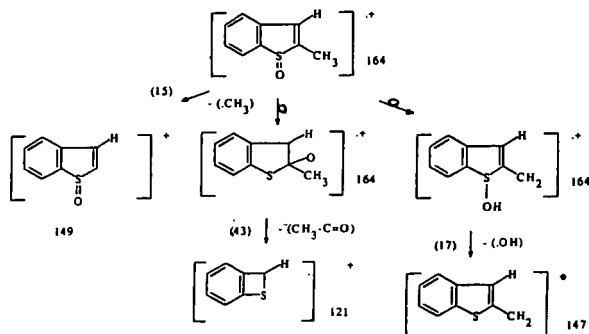


Fig.5 Probable mass fragmentation of methyl benzothiophene, S-oxide.

## HYDROGEN SULFIDE: AN EFFECTIVE REAGENT FOR REDUCING THE ELEMENTAL MERCURY CONTENT OF LIQUID HYDROCARBONS.

by

Costi A. Audeh

Central Research Laboratory  
Mobil Research and Development Corporation  
P. O. Box 1025  
Princeton, NJ 08543-1025

### Abstract

Elemental mercury has been identified in various crude oils and in condensates associated with the production of natural gas. When these liquid hydrocarbons are distilled or further processed, the elemental Hg will appear somewhere in the downstream processes. In cases where downstream equipment contains metals which amalgamate with Hg, the presence of liquid elemental Hg can cause Hg induced stress corrosion which could cause equipment failure.

We have found that the Hg concentration in liquid hydrocarbons, exemplified by a natural gas condensate containing about 120  $\mu\text{g}/\text{Kg}$ , i.e., parts per billion (ppb) Hg, can be reduced to 10-20 ppb. This is accomplished by contacting the condensate with a carrier gas containing 200-500 parts per million of hydrogen sulfide. Typically, the gas containing hydrogen sulfide is mixed with the hydrocarbon containing elemental Hg and passed downflow over a packed bed. Typical reaction conditions are 150°C at a pressure of about 250 psia and a gas to liquid volumetric treating ratio of less than 2:1.

Because the amount of Hg in the condensate used was in the ppb range, it was not possible to recover any HgS for positive identification. However, it is believed that because the stainless steel filter used to filter the treated product acquired a red deposit, and since Cinnabar is the red HgS salt, it is reasonable to conclude that HgS is the product of the reaction.

## INTRODUCTION

Some crude oils [1,2] and natural gas produced in various geographic locations [3,4] contain elemental Hg. In many of the gas producing fields, condensate is also produced in association with the gas. Typically if the gas produced contains Hg, the condensate recovered also contains Hg.

In the U. S., condensates are a valuable source of light distillates for the gasoline market [5]. About 500,000 bbl/day of condensate are used as refinery feedstock [6] and about 15,000 bbl/day in steam cracking for ethylene production [7]. In either application, the Hg in the condensate will have to appear somewhere in the downstream processes. Thus, it would seem that the fate of the Hg will be of concern. This is especially so in the case of steam cracking for ethylene production where equipment made of aluminum is used for cryogenic separation of the cracked products. Any elemental Hg contained in the cracked products is undesirable and could cause Hg induced stress corrosion. Similarly, stress corrosion could also be induced in other process equipment constructed of metals that have the ability to form amalgams.

To prevent Hg carryover and thus the potential corrosion of susceptible process equipment, it is desirable to remove elemental Hg from condensate. In this paper, we report the results of laboratory experiments using hydrogen sulfide as the agent for converting H<sub>2</sub> into HgS.

## EXPERIMENTAL

- 1) Materials: a condensate containing about 120 µg/Kg, i.e., parts per billion (ppb) Hg. Nitrogen gas, methane gas, methane containing about 200 parts per million (ppm) hydrogen sulfide and carbon dioxide gas containing about 480 ppm hydrogen sulfide and about 2.5% methane.
- 2) Equipment: a down flow stainless steel reactor equipped with a mixing T, a preheat zone, temperature control, pressure control, a 1 ml section packed with 10-18 mesh Vycor chips, a 0.7 micron stainless steel product filter and appropriate liquid and gas flow controllers. Figure 1 is a schematic of the reactor and its ancillary systems.
- 3) Procedure:
  - a) Unit start up: from room temperature the gas flow and liquid flow were started and set at the required flow rates. The reactor was heated until the required temperature was reached. After about 10 minutes of steady operation, the product was collected periodically and sampled for Hg analysis.
  - b) Change of conditions: when changes in the process parameters or treating gas were made, the unit was not shut down. It was allowed to equilibrate at the desired conditions and after about 10 minutes of steady operation sampling/testing was resumed.
  - c) Hg determination: this was performed using the Jerome Hg Analyzer, Model 301.

## RESULTS AND DISCUSSION

Hg reacts with  $H_2S$  to produce  $HgS$  and  $H_2$ . Although the solubility of elemental Hg in various hydrocarbons [9] has been reported, that for  $HgS$  has not. However, the solubility of  $HgS$  in water is reported to be  $2.8E-23$  g  $HgS$ /liter of water [10]. Since, in general, inorganic salts are more soluble in water than in hydrocarbons, it would be expected that  $HgS$  will be less soluble in the hydrocarbon condensate used than it is in water. Thus, the solubility of  $HgS$  in the treated condensate is expected to be less than  $2.8E-23$  g  $HgS$ / Kg of condensate. Any  $HgS$  formed would not dissolve to any measurable extent in the treated condensate and possibly, could be removed from the treated product by filtration. Changes in the concentration of Hg in the concentrate will indicate its removal and thus the measure of the effectiveness of this approach is the reduction in the concentration of elemental Hg in the treated condensate.

In the reaction of Hg with  $H_2S$ , each mol of Hg requires 1 mol of  $H_2S$ . Since the concentration of Hg in the feed is about 120 ppb, the amount of  $H_2S$  required to react with it will be very small. Thus we decided to use carrier gases containing small amounts of  $H_2S$  in this study. The gases chosen were methane and carbon dioxide. Methane is the major component of natural gas and natural gas usually contains small amounts of  $H_2S$ . Also, in natural gas processing typically  $CO_2$  and  $H_2S$  are removed from the gas before it can be marketed. In such removal processes, the treating solutions are regenerated and the gases leaving the regenerators contain  $CO_2$  and  $H_2S$ . With this in mind methane/ $H_2S$  and  $CO_2$ / $H_2S$  mixtures were selected for this study.

### "Treating" with Carrier Gas

To determine if "treating" the condensate in the presence of a carrier gas changes the Hg concentration, experiments in which nitrogen and methane without  $H_2S$  were conducted at different temperatures and flow rates. In all cases no significant changes in the Hg content of the treated condensate were observed. From these observations it was concluded that heating the condensate in the presence of a carrier gas does not reduce the Hg content of liquid hydrocarbons.

### Treating the Condensate with $H_2S$ in Methane

Based on the concentrations of the 2 reactants, 200 ppm  $H_2S$  in methane, and 120 ppb Hg in the condensate, it can be shown that  $H_2S$  is in a large molar excess at any reasonable treating ratio. For example, when 1 volume of the treating gas is used to treat 1 volume of the condensate, the  $H_2S$  is in about a 20 molar excess.

- a) **Effect of Temperature** - At a gas to liquid treating ratio of 1:2.7, the treating efficiency increases as the treating temperature is raised. Table 1 shows our results. A plot of  $\ln$  of the concentration of Hg, in ppb, in the treated liquid after treatment vs  $1/T$ , in  $^{\circ}K$ , Fig. 2, gives the straight line:

$$\ln \text{ppb} = 1089 t + 0.95, \text{ where } t = 1/T.$$

- b) **Effect of Feed Ratio** - To study the effect of feed ratio on the efficiency of Hg removal, we varied the rate at which the condensate was pumped and kept the flow rate of the treating gas constant. At 150°C, the temperature chosen for this study, we found that at a treating ratio of about 1:1, the concentration of Hg in the treated condensate approaches about 10 ppb. The results of this study are shown in Table 2.

#### Treating the Condensate with H<sub>2</sub>S in CO<sub>2</sub>

Not unexpectedly, H<sub>2</sub>S/CO<sub>2</sub> was also effective in reducing Hg from the condensate. Table 3 shows our results. At 150°C and a treating ratio of 1:1, the concentration of Hg in the treated condensate approached about 10 ppb.

This study was conducted at a constant temperature 150°C, and a constant gas flow rate, 23 ml/min, but at different condensate feed rates, 10-80 ml/min. Thus, from a plot of the reciprocal of the liquid hourly space velocity, LHSV, vs ln of the concentration of Hg, in ppb, in the treated condensate, Fig. 3, the rate equation, shown below, for the reaction between H<sub>2</sub>S and Hg, can be derived.

$$\ln \text{ppb} = -78.4 v + 4.75, \text{ where } v = 1/\text{LHSV}$$

The slope of this equation gives the rate constant of the reaction in units of ln ppb Hg/hour.

#### Reaction Product

Because the amount of Hg in the condensate is in the ppb range, it was not possible to recover any HgS for positive identification. However, it is believed that because the stainless steel filter used to filter the treated product acquired a red deposit, and since Cinnabar is the red HgS salt, it is reasonable to conclude that HgS is the product of the reaction.

#### CONCLUSION

Laboratory results indicate that H<sub>2</sub>S is an effective reagent for reducing the Hg content of hydrocarbon liquids. In this study, hydrocarbon liquids are exemplified by a condensate produced in association with natural gas and the H<sub>2</sub>S is introduced in about 200-500 ppm in methane or carbon dioxide. At 150°C and about 180 seconds contact time, the Hg content of a condensate containing 120 ppb Hg can be reduced to about 10 ppb.

## REFERENCES

1. Gorbunova, L. V., Filimonova, V. A., Aleshin, G. W., Glokhov, G.G. and Kamyarov, V. F., *Petroleum Chemistry, U.S.S.R.*, Vol. 24, No. 1, p. 10, 1984.
2. Valkovic, V., "Trace Elements in Petroleum", Petroleum Publishing Company, Tulsa, Oklahoma, p.78, 1978.
3. Bodle, W. W., Attari, A. and Serauskas, R., Sixth International Conference on Liquefied Natural Gas, April 7-10, 1980, Kyoto, Japan.
4. Naklie, M. M., Deraton, L. A. and Kartiyoso, Iv., *Oil and Gas Journal*, Vol. 85, No.24, p.35, 1987.
5. Staff Report, *Oil and Gas Journal*, V. 84, No. 2, p. 71, 1986.
6. S. R. I. Chemical Economics handbook, 229.3000Z.
7. *ibid.*, 300.5201A.
8. Kelley, K. K. *Bur. of Mines Bull.*, 1937, No. 406, 52
9. Spencer, J. N. and Voigt, A., *J. Phys. Chem.* V. 72, p. 464, 1968.
10. Linke, W. F., "Solubilities" Volume 1, Van Nostrand, Washington, D. C., 1958, p. 1249.

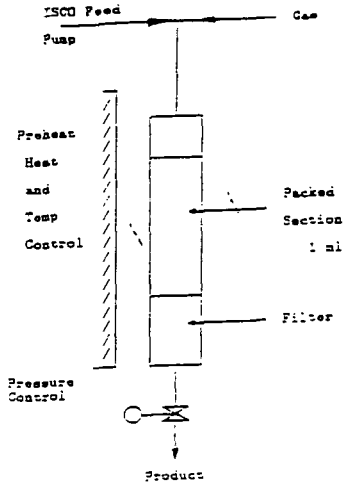


FIGURE 1  
REACTOR FOR Hg REMOVAL

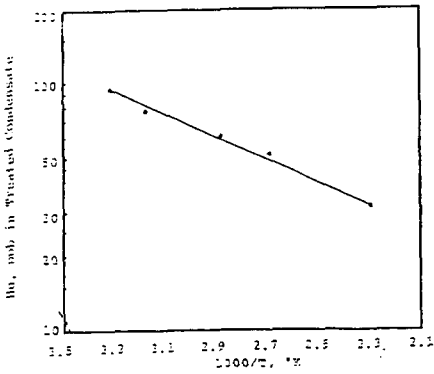


FIGURE 2  
EFFECT ON FEED RATIO ON Hg REMOVAL

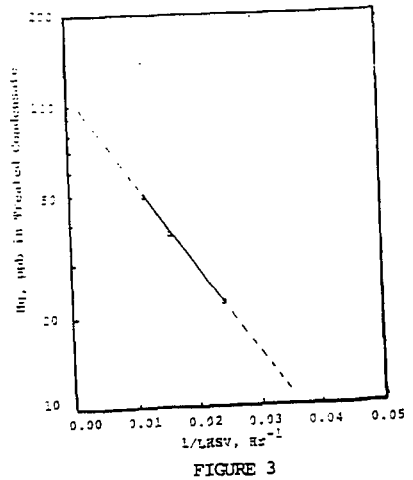


FIGURE 3  
EFFECT ON FEED RATIO ON Hg REMOVAL

**TABLE 1****Removal of Hg from Condensate (C) with H<sub>2</sub>S in CH<sub>4</sub>  
Effect of Temperature**

Gas: 200 ppm H<sub>2</sub>S/balance CH<sub>4</sub>  
 Packing: 1 ml 10-18 mesh Vycor chips  
 Pressure: 220-260 psig

<u>Temperature</u> °C	<u>Volume ml/hr</u> (C) CH <sub>4</sub> /H <sub>2</sub> S		<u>Hg in Product</u> ppb	<u>Hg Removed</u> %
	Feed	----	116	----
29	70	26	95	19
43	70	26	77	34
75	70	26	60	49
100	70	26	52	55
165	70	26	31	74

**TABLE 2****Removal of Hg from Condensate (C) with H<sub>2</sub>S in CH<sub>4</sub>  
Effect of Feed Ratio**

Gas: 200 ppm H<sub>2</sub>S/Balance CH<sub>4</sub>  
 Packing: 1 ml 10-18 mesh Vycor chips  
 Pressure: 220 - 260 psig  
 Temperature: 150 °C

<u>Volume ml/hr</u> (C) CH <sub>4</sub> /H <sub>2</sub> S		<u>Hg in Product</u> ppb	<u>Hg Removed</u> %
Feed	---	116	----
80	26	52	54
30	26	34	70
52	26	28	78
40	26	23,20,21	82
13	26	<10	>90

**TABLE 3**

**Removal of Hg From Condensate (C) with H<sub>2</sub>S in CO<sub>2</sub>  
Effect of Condensate to Gas Ratio**

Gas: 500 ppm H<sub>2</sub>S/2.5% CH<sub>4</sub>/balance CO<sub>2</sub>  
Packing: 1 ml 10-18 mesh Vycor chips  
Pressure: 220-260 psig  
Temperature: 150 °C

<u>Volume, ml/hr</u> <u>(C) CO<sub>2</sub>/H<sub>2</sub>S</u>	<u>Hg in Product</u> <u>ppb</u>	<u>Hg Removed</u> <u>%</u>
Feed ----	116	----
80 23	50,47	58
60 23	38,36	68
40 23	17,21,19	84
20 23	<10,11,<10	>90
10 23	<10,<10,<10	>90

**EFFECT OF LIGNITE PROPERTIES AND ASH CONSTITUENTS  
ON THE HYDROLIQUEFACTION BEHAVIOR OF THE TURKISH LIGNITES**

M. Oner, E. Bolat, G. Yalin, S. Dincer  
Yildiz Technical University  
Chemical Engineering Department  
Istanbul, TURKEY

**Keywords:** lignite properties, hydroliquefaction, ash

**INTRODUCTION**

In Turkey, coal represents major non-renewable energy resources since lignite and bituminous coal reserves are known to be around 8.1 billion tons and 1.4 billion tons, respectively. The high demand for imported fuel oil for energy requirement of Turkey has led to strong and sustained interest in the prospects for producing liquids from the coal resources. Due to the high sulfur (1-5 %), ash (10-50 %), moisture (10-40%) and low calorific value of Turkish lignites, coal liquefaction processes is believed to be one of the efficient way by converting them to clean liquid fuels and chemical feedstocks.

The purpose of this study was to develop correlations between physical, chemical and petrographic properties of representative Turkish lignites and liquefaction yield data obtained in tetralin, anthracene, creosote and vacuum residue oils, with or without catalyst, at 440 °C and 80 bar hydrogen pressure (cold charge).

**EXPERIMENTAL**

**Materials and Procedure**

Experiments were carried out by BE (Beypazari), CA (Can), EL (Elbistan), IL (Ilgin), KN (Kangal), KR (Karliova), SA (Saray), SE (Seyitomer), SO (Soma), TU (Tuncbilek), YA (Yatagan) lignites using tetralin, Tupras vacuum residue oil, anthracene and creosote oils as solvents. Creosote and anthracene oils used in this study were obtained from Karabuk Demir Celik Fabrikalari A.S. and vacuum residual oil (VR) was provided by Tupras, Turkey. Tetralin was supplied by Merck company and it was used as received. The creosote oil used has a carbon to hydrogen ratio of 1.24 (90.78% C, 6.12% H, and 0.70% N); anthracene oil has a carbon to hydrogen ratio of 1.27 (91.50% C, 6.01% H, and 0.75% N); vacuum residue oil has a carbon to hydrogen ratio of 0.64 (85.58% C, 11.06% H and 0.50% N). Two catalysts were used in these experiments. A commercially available alumina supported CoMo (3% CoO and 10% MoO<sub>3</sub> on Al<sub>2</sub>O<sub>3</sub>) was used in extrusion form having 2.6-3 mm diameter and bulk density of 0.5-0.6 kg/lit. In addition, a disposable catalyst, red mud (15.03% SiO<sub>2</sub>, 35.96% Fe<sub>2</sub>O<sub>3</sub>, 21.04% Al<sub>2</sub>O<sub>3</sub>, 4.56% TiO<sub>2</sub>, 9.3% Na<sub>2</sub>O and 3.5% CaO) received as a waste by-product of Seydisehir Aluminum Company, having a grain size of 0.01 mm, was used. The elemental analysis for carbon, hydrogen and nitrogen was done by Beller Microanalysis Laboratories in Germany. The ash samples prepared at 800 °C were analyzed with Inducted Coupled Plasma (ICP) Leeman, Model PS1000 series.

The liquefaction experiments were carried out in a 250 ml magnetically stirred and electrically heated stainless steel autoclave manufactured by Ernst Haage. Based on the literature and evaluation of our previous work, the reaction temperature, pressure and reaction time for these experiments were chosen as 440 °C, 80 bar hydrogen (cold charge), respectively (1-3). Solvent/lignite or asphaltite ratio was chosen as 2 (db). At the completion of a liquefaction experiment, the autoclave was cooled overnight to room temperature and the gases were analyzed by Shimadzu Moduline GC-9A model gas chromatography. The liquid products and solid residue washed from the autoclave with toluene and fractionated by Soxhlet extraction into oil (hexane soluble

material); asphaltene (toluene soluble, hexane insoluble material); preasphaltane (tetrahydrofuran (THF) soluble, toluene insoluble material); and residue (THF insoluble material). The blank runs for all sets of experiments with no lignite present were carried out with all solvents to evaluate the reactivity of the lignite samples.

## RESULTS AND DISCUSSION

The complete experimental data were reported in previous work (1-3). The characterization data for the lignites used are given in Tables 1 and 3. The experimental data used in this study are given in Figures 1-2.

The intercorrelation of experimental results and lignite characteristics was evaluated by simple linear regression analysis using Microstat Statistical Package program. By the application of simple linear regression, it was found that generally a good correlation did not exist between individual lignite properties and yield and conversion data. Only total sulfur content and xylene extract of lignites were observed to give partially acceptable correlations for the oil yields. The correlation coefficient of experiments using tetralin as solvent is as follows:

$$O (\% \text{ daf}) = 3.10 S_t + 50.84 \\ R^2 = 0.7024 ; \text{SEOE}(\text{standard error of estimation}) = 4.45$$

The oil yields obtained in experiments using creosote oil and red mud catalyst were correlated with xylene extract content of lignites by the following regression equation

$$O (\% \text{ daf}) = 1.980 \text{XEL} + 29.39 \\ R^2 = 0.560 ; \text{SEOE} = 6.68$$

The effect of individual coal properties are not easily assessed as noted above. This is primarily due to the fact that the individual properties being highly cross-correlated hence they could not be independently varied. Therefore, the multiple regression analysis was employed and in order to improve the correlation coefficients unfitting lignites were eliminated. The equations developed with oil yield as the dependant variable are given in Table 4. The correlation coefficients indicated that a relationship existed between carbon, total sulfur and forms of sulfur, volatile matter, huminite plus exinite, and xylene extract of lignites with the oil yields obtained by using four different solvents and two different catalysis. The highest correlation coefficient was obtained for experimental data using creosote oil as the solvent. For this case three equations were derived, using the pyritic sulfur, total sulfur and organic sulfur contents of the lignites. The  $R^2$  values are 0.6819, 0.9727 and 0.7643 for  $S_p$ ,  $S_t$ , and  $S_o$ , respectively as shown in Equations 2-4. It is commonly believed that one of the factors contributing to the liquefaction yield is promotion by sulfur. However, the exact role of sulfur is not well understood. The organic sulfur is presumably present in coal as mercaptans, sulfides, thioethers. It is expected that thioethers are thermally cleaved at considerably low temperature to produce active coal fragments during the liquefaction reactions (4). Several workers have shown that conversion of coals of low sulfur content can be increased by from 5 to 18 percent through the addition of pyrite (5,6). It has been observed that during liquefaction, pyrite is reduced to pyrrohotite and hydrogen sulfide at roughly the same rate as the organic matter is converted to liquid products. Thus coals containing high proportions of pyritic sulfur will tend to form pyrrohotites with a high level of iron vacancies, which appear to promote liquefaction.

There is an indication that an increase in ash, huminite plus exinite, xylene extract and volatile matter contents of lignites help the hydroliquefaction process positively. On the other hand, as the negative coefficient before the elemental carbon content in Eq.5 indicates, increasing the elemental carbon content decreases the oil yield. As shown in equations 2-4 and 6-7, correlations were obtained when HU and

HU+EX contents of the lignite were used as the petrographic correlating parameter. The work undertaken by Given and coworkers in batch reactor showed that some coal macerals, including vitrinite, pseudovitrinite and liptinites are reactive while inertinite, as its name implies, is inert in coal liquefaction (7). The trend for increasing reactivity with increasing volatile matter content as given in Equations 2-4 was expected as volatile matter is known to be thermally easily liberated. Given also found that volatile matter had a direct correlation with conversion at 60 minutes and exhibited the highest correlation coefficient among the coal properties investigated (7). The oil yield increases as the xylene extract content of the lignite increases, as seen in Equations 1-4 and 7-8. The high partial correlation coefficients for xylene extract in Equations 2-4 indicate that it may be considered as a good correlation parameter for liquefaction reactions.

The equations 1, 6 and 8 show that increased ash content increases oil yield. It is known that the high ash coals are more easily hydrogenated than low ash coals because certain coal ash minerals catalyze the reactions (8-9). The observed relation between ash and oil yield data was further evaluated with respect to concentrations of ash constituents (g/100g of inorganic matter). In this study total Fe, Al, Si, Mg, Ca, Na and K concentrations were chosen as the independent variable, since the active form of the minerals has not been ascertained. There appears to be direct correlation between oil yield with Fe constituents but the dependence is not marked. The yield of oil data shows a tendency to increase with increasing Al, Ca and Mg content though with more scatter than in the case of Fe content. No detectable trends were observed with Si contents of ash. In this study, an examination of oil data for all samples studied did not reveal any statistically significant correlations with Na and K content of the ash. We have not included in this paper a thorough discussion for the effects of ash constituents on liquefaction yields because we are carrying out a detailed multiple regression analysis on that topic.

#### CONCLUSIONS

In this study, the oil yields of the Turkish lignites under same hydroliquefaction conditions in the presence of tetralin, creosote, anthracene and vacuum residue oils using a catalyst or not, were correlated total, pyritic and organic sulfur, volatile matter, elemental carbon, huminite, huminite plus exinite, xylene extract, ash and ash constituents of lignites using simple and multiple linear regression analysis. The derived equations indicated that although use of different lignite, solvents and catalyst resulted in different yield data, the oil yields exhibit almost similar dependencies on lignite characteristics. However, it should be noted that in order to strengthen the validity of these equations, the number of lignite sample studied should be increased. In any case, much more has to be done in order to correlate the liquefaction data with lignite properties.

#### REFERENCES

1. Oner, M., Bolat, E., Dincer, S., *Energy Sources*, 12, 407, 1990.
2. Oner, M., Bolat, E., Dincer, S., *Energy Sources*, 14, 81, 1992.
3. Bolat, E., Oner, M., Yalin, G., Dincer, S., *Fuel Science and Technology International*, 31, 55, 1992.
4. Miller, R. L., and Baldwin, R.M., *Fuel*, 64, 1235, 1985.
5. Alexander, B.F. and Anderson, R.P., *Div. Fuel Chem. Amer. Chem. Soc., Prepr.*, 27(2), 18, 1982.
6. Bockrath, B.C. and Schroeder, K.T., in "New Approaches in Coal Chemistry", eds. B.P. Blaustein et al., ACS Sym. Series 169, 191, 1981
7. Given, P.H., Cronauer, D.C., Spackman, W., Lowell, H.L., Davis, A., and Biswas, B., *Fuel*, 54, 40, 1975.
8. Mukherjee, D.K., Choudhury, P.B., *Fuel*, 55, 4, 1976.
9. Guin, J.A., Tarrer, J.M., Lee, J.M., Van Brackie, H.F., Curtis, C.W., *Ind. Eng. Chem. Proc. Des. Dev.*, 18(4), 631, 1979.

Table I  
Analytical Data for Lignites Used

Lignite Sample	C (%daf)	H (%daf)	N (%daf)	S <sub>t</sub> (%dry)	S <sub>o</sub> (%dry)	S <sub>p</sub> (%dry)	S <sub>o</sub> (%dry)	S <sub>p</sub> (%dry)	VM (%daf)	FC (%daf)	ash (%dry)	H/C (Atomic)	XEL (%daf)
BE	64.90	5.61	2.19	5.69	2.33	2.88	2.33	0.48	35.61	64.38	49.88	1.04	3.83
CA	66.38	4.82	1.67	4.23	2.44	0.90	2.44	0.89	37.53	62.47	27.15	0.87	1.34
EL	65.95	4.97	2.48	5.82	2.22	3.33	2.22	0.27	54.78	45.22	28.19	0.90	5.04
IL	68.19	5.11	1.27	2.95	1.45	1.12	1.45	0.38	40.32	59.68	33.61	0.90	5.69
KN	67.66	4.52	2.78	5.63	1.93	3.15	1.93	0.55	62.93	37.07	38.50	0.80	5.22
KR	66.97	5.55	2.09	0.79	0.30	0.40	0.30	0.09	49.43	50.57	49.20	0.99	4.31
SA	61.32	4.73	1.60	4.97	1.25	0.15	1.25	3.57	48.21	51.79	59.99	0.93	12.62
SE	71.97	4.70	2.32	1.45	1.02	0.26	1.02	0.17	48.65	51.35	24.87	0.78	10.30
SO	64.10	5.62	1.47	0.80	0.34	0.41	0.34	0.05	39.69	60.30	55.51	1.05	2.02
TU	78.30	5.65	3.03	1.37	0.64	0.64	0.64	0.06	31.59	68.41	18.59	0.87	0.95
YA	65.65	4.87	1.59	5.11	2.98	1.72	2.98	0.41	44.41	55.59	25.35	0.92	6.90

BE: Beypazari; CA: Can; EL: Elbistan; IL: Ilgin; KN: Kangal; KR: Karliova; SA: Saray; SE: Seytomer; SO: Soma;

TU: Tuncbilek; YA: Yatagan; S<sub>t</sub>: total sulfur; S<sub>o</sub>: pyritic sulfur; S<sub>p</sub>: organic sulfur; S<sub>o</sub>: sulfatic sulfur;

VM: volatile matter; FC: fixed carbon; daf: dry-ash-free; XEL: Xylene extract of lignites.

Table II  
Maceral Group Analysis of Lignites

Lignite	Maceral Group Analysis (volume %)					Organic Based Maceral Group Analysis (volume %)		
	Huminites (HU)	Exinites (EX)	Inertinites (IN)	Pyrites	Clays	Huminites (HU)	Exinites (EX)	Inertinites (IN)
BE	77	6	4	3	10	88	7	5
CA	74	6	4	4	12	88	7	5
EL	69	5	11	3	12	81	6	13
IL	70	7	9	3	11	81	8	11
KN	54	4	7	3	32	83	6	11
KR	52	5	7	2	34	81	8	11
SA	71	6	7	2	14	85	7	8
SE	77	7	8	2	6	84	8	8
SO	62	3	9	2	24	84	4	12
TU	80	8	6	1	5	85	9	6
YA	77	6	5	4	8	88	7	5

Table III  
Chemical Analysis of Ash (g/100 g organic matter)

Lignite	Si	Fe	Al	Mg	Ca	K	Na
BE	22.06	6.70	6.60	2.59	6.89	1.14	3.54
CA	8.24	3.26	5.55	0.13	1.18	0.27	0.12
EL	5.47	1.45	2.69	0.74	6.87	0.20	0.12
IL	9.36	2.88	6.88	0.96	3.75	1.60	2.06
KN	11.35	1.69	7.20	0.84	8.64	0.52	0.29
KR	33.26	3.70	3.97	0.81	2.34	2.44	0.42
SA	32.55	14.42	18.19	4.03	5.49	2.88	0.40
SE	9.02	6.87	1.94	1.12	2.18	0.13	0.34
SO	27.65	3.64	17.80	1.07	8.05	1.50	0.46
TU	5.48	2.29	3.52	0.47	0.37	0.27	0.03
YA	4.30	3.28	2.97	0.54	4.23	0.25	0.07

Table IV

Relations Between Oil Yield and Various Properties of Turkish Lignites

Solvent + Catalyst Used	Excluded Lignite	Derived Equation	Eq (1) SEOE = 5.74
A.O.	SE, BE	$O (\% \text{daf}) = 20 + 0.44 \text{ ash} + 1.17 \text{ XEL}$ $R^2 = 0.7719$ $R_{\text{ash}}^2 = 0.5598$ $R_{\text{XEL}}^2 = 0.3501$	Eq (1) SEOE = 5.74
C.O.	SO, TU	$O (\% \text{daf}) = -247.4 + 1.41 S_p + 0.18 \text{ VM} + 2.00 \text{ XEL} + 2.93 (\text{HU} + \text{EX})$ $R^2 = 0.9890$ $R_{S_p}^2 = 0.6819$ $R_{\text{VM}}^2 = 0.4644$ $R_{\text{XEL}}^2 = 0.9890$ $R_{(\text{HU} + \text{EX})}^2 = 0.6819$	Eq (2) SEOE = 1.36
		$O (\% \text{daf}) = -223.1 + 0.99 S_p + 0.17 \text{ VM} + 1.79 \text{ XEL} + 2.66 (\text{HU} + \text{EX})$ $R^2 = 0.9991$ $R_{S_p}^2 = 0.9727$ $R_{\text{XEL}}^2 = 0.9977$ $R_{(\text{HU} + \text{EX})}^2 = 0.9967$	Eq (3) SEOE = 0.40
		$O (\% \text{daf}) = -216.1 + 2.32 S_p + 0.20 \text{ VM} + 1.89 \text{ XEL} + 2.56 (\text{HU} + \text{EX})$ $R^2 = 0.9918$ $R_{S_p}^2 = 0.7643$ $R_{\text{XEL}}^2 = 0.9900$ $R_{(\text{HU} + \text{EX})}^2 = 0.9645$	Eq (4) SEOE = 1.17
TET	EL, SO	$O (\% \text{daf}) = 125.1 - 0.97 C + 1.82 S_p$ $R^2 = 0.9039$ $R_C^2 = 0.8697$	Eq (5) SEOE = 2.12
VR	BE, KN	$O (\% \text{daf}) = 29.22 + 0.09 \text{ Ash} + 0.30 \text{ HU}$ $R^2 = 0.4800$ $R_{\text{ash}}^2 = 0.4169$ $R_{\text{HU}}^2 = 0.3999$	Eq (6) SEOE = 1.61
C.O. + CoMo	KR, KN	$O (\% \text{daf}) = -61.62 - 1.22 \text{ XEL} + 1.18 (\text{HU} + \text{EX})$ $R^2 = 0.5704$ $R_{\text{XEL}}^2 = 0.4904$ $R_{(\text{HU} + \text{EX})}^2 = 0.3512$	Eq (7) SEOE = 5.70
C.O. + Red Mud	KR	$O (\% \text{daf}) = 25.25 + 0.20 \text{ Ash} + 1.67 \text{ XEL}$ $R^2 = 0.7908$ $R_{\text{ash}}^2 = 0.3286$ $R_{\text{XEL}}^2 = 0.7091$	Eq (8) SEOE = 4.42

A.O.: Anthracene oil; C.O.: Creosote oil; TET: Tetralin; VR: Vacuum residue; CoMo: Cobalt Molybdenum catalyst.

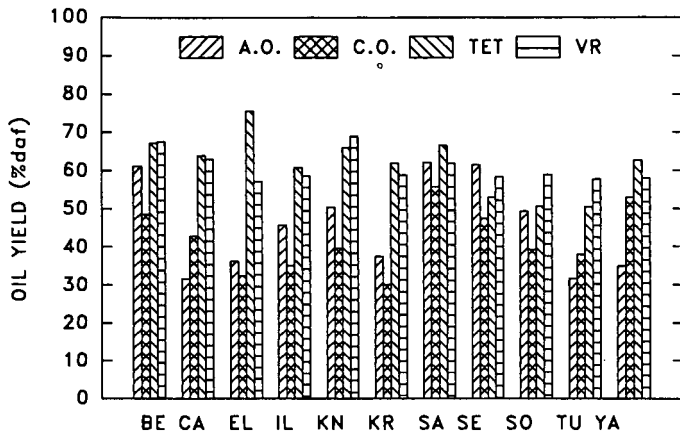


Figure 1. Effect of solvents on the oil yields of Turkish lignites; P = 80 bar (H<sub>2</sub>, cold charge), T = 440 °C, reaction time = 1 hr.

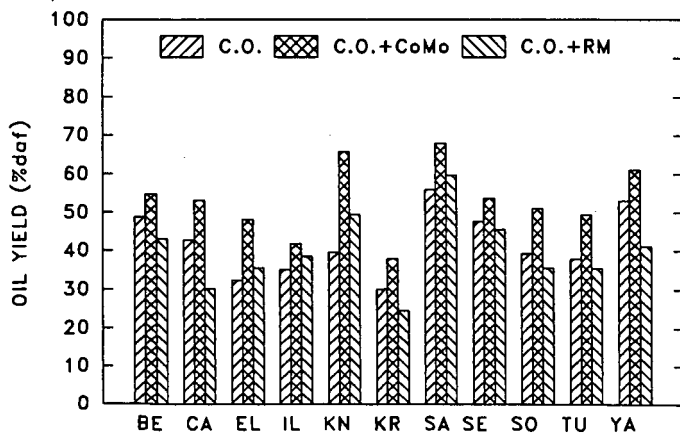


Figure 2. Effect of catalysts on oil yields of Turkish lignites; P = 80 bar (H<sub>2</sub>, cold charge), T = 440 °C, reaction time = 1 hr.